MECHANICAL CHARACTERIZATION OF ADVANCED POLYACRYLONITRILE DERIVED CARBON FIBERS REINFORCED WITH CARBON NANOTUBES

BY

NICHOLAS FASANELLA

THESIS

Submitted in partial fulfillment of the requirements
for the degree of Master of Science in Aerospace Engineering
in the Graduate College of the
University of Illinois at Urbana-Champaign, 2012

Urbana, Illinois

Adviser:

Associate Professor Ioannis Chasiotis, Director of Research

ABSTRACT

This research focused on the mechanical characterization of individual carbon fibers reinforced with carbon nanotubes (CNTs) which were dispersed in the polyacrylonitrile (PAN) precursor. The carbon nanofibers were obtained from the Georgia Institute of Technology and were fabricated in bundles by the "islands-in-a-sea" method. The fiber test specimens, with roughly 1 μm in diameter and 50 or 100 μm in gauge length, were tested in tension by specially designed MEMS devices that provided independent measurement of fiber force and extension with the aid of digital image correlation (DIC). The fiber extension and force data were used to derive stress vs. strain plots for a large number of individual fibers. The *two* parameter Weibull distribution was used to analyze the mechanical strength data. Due to variability in the fiber cross-section and the *two* different gauge lengths, a volume corrected Weibull analysis was applied.

Fibers isolated from three different bundles, all subject to the same manufacturing conditions, were tested. The first fiber bundle yielded an average tensile strength of 3.41±0.93 GPa, Young's modulus of 228±45 GPa, and Weibull characteristic strength of 4.3 GPa. The second data set, comprised of fibers from the third bundle, resulted in average tensile strength of 4.55±1.35 GPa, Young's modulus of 254±36 GPa, and Weibull characteristic strength of 5.07 GPa. A third data set was generated with carbon fibers from bundles #2 and #3 by using compliant gripping that prevented failure at the specimen grips resulted in an average tensile strength of 5.59±1.24 GPa. The strongest fibers from the first, second and third data sets had tensile strengths 5.66 GPa, 7.24 GPa, and 7.31 GPa, respectively. All fiber bundles provided strength values that were significantly higher than those reported for the control carbon fiber manufactured under the same conditions but without CNTs.

ACKNOWLEDGEMENTS

I am very grateful to my advisor, Prof. Chasiotis, for his guidance, support, and for giving me the opportunity to work on this project. I would like to thank DARPA and the Army Research Office Grant #W911NF-10-1-0098 for providing me the necessary funding to conduct this research. I would also like to thank Prof. Kumar and his group at the Materials Science and Engineering Department of the Georgia Institute of Technology for providing the samples researched in this study. I also extend my thanks to the entire staff of the Aerospace Engineering Department at UIUC for their invaluable assistance in any administrative issues.

I would like to express a very special thanks to Mr. Korhan Şahin, who was my colleague on this project and acted as a friend and mentor throughout the study. I would also like to extend my thanks to my colleagues in the Nanomechanics Research Lab, namely Tanil, Ankit, Pavan, Nikhil, Siva, Jan and Debashish, for their assistance, support, and friendship throughout the duration of this study. I gratefully acknowledge the staff members at MRL who trained and assisted me on the FEI Dual Beam 235 FIB and SEM instruments. Finally, I am extremely thankful for my parents and the rest of my family and friends. Without their constant love and support I could have never had the opportunity to write this thesis.

TABLE OF CONTENTS

CHAPTER 1

INTRODUCTION

Carbon fibers are among the most highly researched materials for aerospace applications due to their outstanding properties. They have higher specific strength and stiffness than other reinforcement fibers [1-3], they exhibit good fatigue resistance [4] and thermal expansion properties [5], they possess good electrical conductivity [6], and they are chemically inert [7]. Carbon fibers can be derived from a number of precursors, the most common being polyacrylonitrile (PAN), petroleum derived pitch, and the cellulose fiber rayon [1,2,6-8], and are widely used in commercial applications [9]. Pitch comes in two types, isotropic pitch and mesophase pitch. PAN is known for its high strength properties, while mesophase pitch is known for its high modulus [10]. Vapor grown carbon fibers (VGCF)s are another type of carbon fiber, with nanoscale radii and very good thermal and electrical properties [11,12].

The highly anisotropic nature of the graphite crystal is in part responsible for the outstanding properties of carbon fibers which can be graphitic, amorphous or turbostratic [13]. In graphite, carbon atoms are arranged in planar layers of hexagonal, honeycomb-like, ABAB stacking [14], as shown in Figure 1.1. The in-plane bond length between atoms is 0.1421 nm and the interplanar separation is 0.3354 nm [15]. The large spacing between graphene planes is responsible to a weaker, van der Waals type interaction rather than covalent bonding [7], which leads to large property anisotropy. In plane atoms are held together by covalent bonds with strength of 400 kJ/mol due to sp^2 hybridization of the electron orbitals [1]. When loaded in the direction labeled “a” in Figure 1.1, which is parallel to the honeycomb planes, a theoretical tensile modulus of 1060 GPa and strength

of 106 GPa have been estimated [16]. However, due to weak van der Waals forces in the out of plane direction, labeled “b” in Figure 1.1, the modulus in this direction is only 36.5 GPa [15]. The extremely high in-plane mechanical stiffness of graphite has made carbon fibers the subject of intensive research.

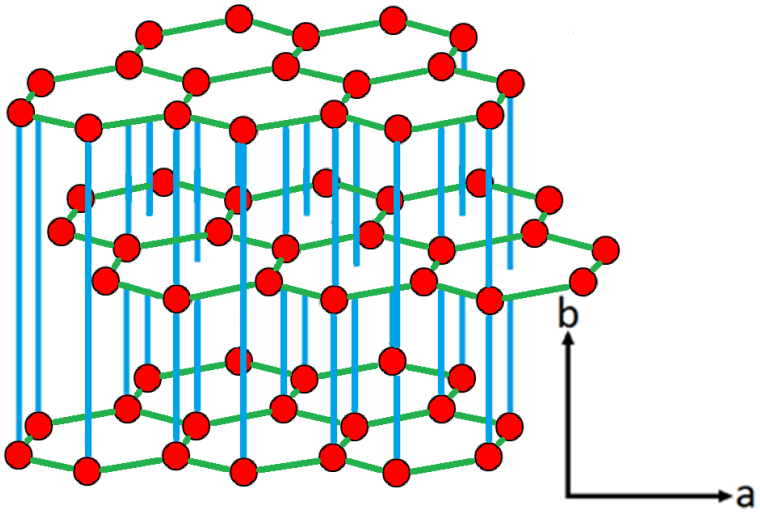

Figure 1.1 Structure of graphite.

The first carbon fibers were produced by Thomas Edison in the late 1800’s. Edison intended these fibers for incandescent light bulbs and manufactured them first by carbonizing bamboo and then from regenerated cellulose, or rayon. In the 1950s carbon fibers made from rayon were used for thermal insulation [8]. The first commercial carbon fibers were produced in the 1960s by the Union Carbide Corporation [16]. Through the use of stress graphitization, the microcrystalline structure of rayon was converted from random to oriented turbostratic carbon [17]. The fibers dubbed VYB and WYB were both created from rayon but subjected to different heat treatments at 1000°C and 2500°C respectively [1]. Due to the relatively low temperature, VYB contained small amounts of non-carbon elements with carbon being isotropic and non-graphitizing [18]. WYB fibers were heated at sufficiently high temperatures to result in pure carbon. Notably, WYB was

incorrectly marketed as a “graphite fiber” to indicate its pure carbon content, despite the fact it did not have a graphitic structure [16].

In the 1960s carbon fibers derived from PAN were developed. Shindo first reported the use of PAN as precursor for carbon fibers [19]. The fibers showed a moderately high modulus of 170 GPa, but low strength values of 550-700 MPa. These low mechanical properties were partially attributed to poor molecular orientation [16]. Phillips, Watt and Johnson developed the first commercial process successfully converting PAN precursor fibers into carbon fibers [20]. It was found that high strength and modulus could be achieved from oriented PAN precursor by applying tension in order to elongate the fibers or prevent shrinkage [21,22]. These fibers were commercialized by Morganite, Ltd. and Courtaulds Ltd. and in 1966 became the first high performance carbon fibers [7]. These PAN-based carbon fibers were designated as type I for high modulus, and type II for high strength.

Since PAN’s introduction, other commercial carbon fibers have been developed. In the mid-1960’s Kureha Chemical Industry Co. Ltd. in Japan began investigating asphaltic, or pitch, materials to use in graphite filaments [23]. The discovery that fibers with true graphitic structure could be created using pitch led to research on pitch as a carbon fiber precursor [24]. Pitch fibers can have extremely high tensile modulus approaching 1,000 GPa [25] which is very close to the aforementioned theoretical modulus for a graphitic fiber. VGCFs are another common type of carbon fiber, manufactured by decomposing a hydrocarbon gas in the presence of a transition metal filament on a heated substrate. The transition metal filament is nucleated by a catalyst and the fiber grows away from the heated substrate [26-28]. Koyama and Endo introduced a continuous process for creating VGCFs, which, after modification, yields fibers with submicron diameters and lengths up to 100 μm [29,30]. Since they are relatively inexpensive, VGCFs have been used as reinforcement in polymer composites [31].

This dissertation focuses on carbon fibers derived from PAN. PAN-based carbon fibers have high carbon yield, as well as good tensile and compressive strength [12]. While the modulus of PAN derived carbon fibers is not as high as those from mesophase pitch, the former have superior strength [25]. Additionally, production of carbon fibers from mesophase pitch is more expensive than from PAN [32]. The first step in producing carbon fibers from PAN is to manufacture the polymer precursor which consists of highly polar nitrile groups, and, therefore, is rarely used as a carbon fiber precursor [25]. In practice, PAN precursor fibers contain 6-9% of other monomers [33,34]. Once the precursor is prepared, PAN fibers can be spun by wet, melt, dry, gel and dry-jet wet spinning [32]. Wet spinning is the most common method and involves polymer extrusion directly in the coagulation bath where the fiber is then drawn [35,36].

The general process for fabricating carbon fibers from various precursors is similar. Here, the process for creating a carbon fiber from PAN precursor is described, but fibers derived from pitch or rayon do not vary greatly. The first step is stabilization at 200-300°C, often done under tension [7,37]. Stabilization converts the polymer precursor to a thermally stable and condensed structure [22,38]. The next step is carbonization in nitrogen atmosphere and at temperatures 1000-1700°C [39] where most of the non-carbon elements are removed. During carbonization, the tensile strength can increase to ~3 GPa, and the tensile modulus to ~250 GPa [40] due to an increase in the degree of crystallinity and improved molecular orientation. A graphitization step can follow in inert atmosphere between 2,000-3,000°C to form a graphitic structure aligned in the fiber direction [7]. It is important to note that the elastic modulus continues to increase with heat treatment, but the maximum strength is reached at ~1500-1600°C [41]. The loss of strength can be attributed to the reduction in nitrogen and, therefore, the formation of flaws [42]. The strength reaches a minimum at ~1800°C when the nitrogen content is virtually zero. After nitrogen is fully removed the lattice defects can rearrange, leading to a second tensile strength peak at ~2400°C, though not as high as the initial peak at ~1500°C [43]. The microstructure of graphitized PAN fibers has graphite layers oriented in the fiber direction that fold over one another by 180° in a hairpin fashion in the

transverse direction [44]. The fibers exhibit a “skin-core” structure where the planes have a circumferential orientation around the cross-section of the fiber [45].

1.1 Nanotube Reinforced Carbon Fibers

CNTs have been researched extensively in the last 20 years due to their outstanding mechanical [46,47], electrical [48-50] and thermal properties [51,52]. CNTs come in various forms, such as single wall carbon nanotubes (SWCNT), double wall carbon nanotubes (DWCNT) and multi-wall carbon nanotubes (MWCNT). As the name indicates, SWCNT are an atom thick single layer of graphene with a cylindrical structure and a diameter of ~1.4 nm [53], although SWCNT with diameter as small as 0.4 nm have been produced [54]. The tensile strength of SWCNT has been cited as 37 GPa, or higher, [55] and the axial elastic modulus as 640 GPa or higher [56]. DWCNT have two layers of concentric cylindrical graphite, with outer diameter of 2-5 nm [57]. MWCNTs consist of many of these graphite layers, and typically range from 5-50 nm in diameter [58].

Fullerenes, or molecules made entirely of carbon, were discovered by Kroto *et. al* in 1985 [59]. In 1991, Iijima of the NEC Laboratory in Japan made the first discovery of MWCNTs [60], which started extensive research on CNTs due to their unique structure. SWCNTs were discovered by Iijima [61] and Betheune *et. al* at the IBM Almaden laboratory [62], while Smalley *et. al.* manufactured aligned bundles of SWCNTs [53]. More recently, the dispersion of CNTs in carbon fiber precursors to act as mechanical reinforcements has been pursued [63]. CNTs were dispersed in a solution of dimethylacetamide by simultaneous stirring and sonication. The solution of PAN and CNTs was spun using dry-jet-wet spinning at room temperature [63]. Figure 1.2 shows the dispersion of various types of CNTs: when the CNTs were well dispersed and aligned with the fiber axis the resulting carbon fibers demonstrated high strength.

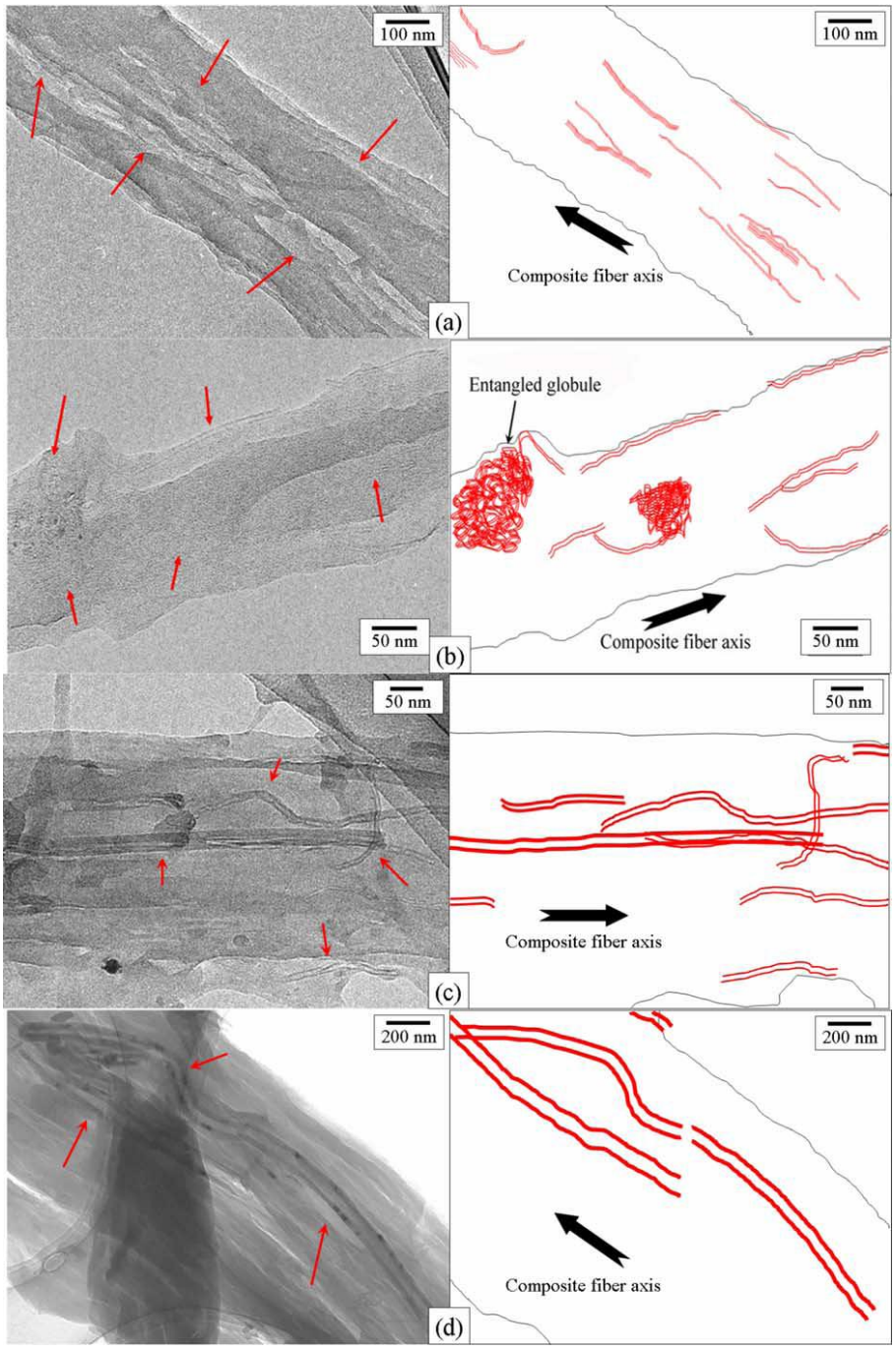

Figure 1.2 Alignment of nanotubes in PAN/CNT composite fibers. **(a)** SWCNTs. **(b)** DWCNTs. **(c)** MWCNTs. **(d)** VGCNTs [63]. Reprinted from *Polymer*, 46 (24) with permission from Elsevier.

Composite gel spun PAN fibers containing 0.5% wt and 1% wt SWCNTs have been fabricated [64] with diameters of 12-13 μm, and 6 μm, respectively. The carbonized (1100°C) PAN/SWNT displayed higher orientation and larger crystallite size than the control. Graphitic structure was present in the vicinity of the CNTs in the PAN/SWNT fibers as shown in Figure 1.3(a-f). On the other hand, the control carbon fibers were comprised of disordered carbon. The 6 μm in diameter PAN/SWNT fibers with 1% wt CNTs displayed 64% increase in tensile strength and 49% increase in the elastic modulus compared to the control. The average tensile strength was 3.2 GPa and the average modulus was 450 GPa [64]. This ability to attain graphitic structure at low temperatures should theoretically allow for high-strength fibers. With the addition of CNTs, substantial and efficient load transfer to the CNTs may further aid in increasing the tensile strength of the composite carbon fibers.

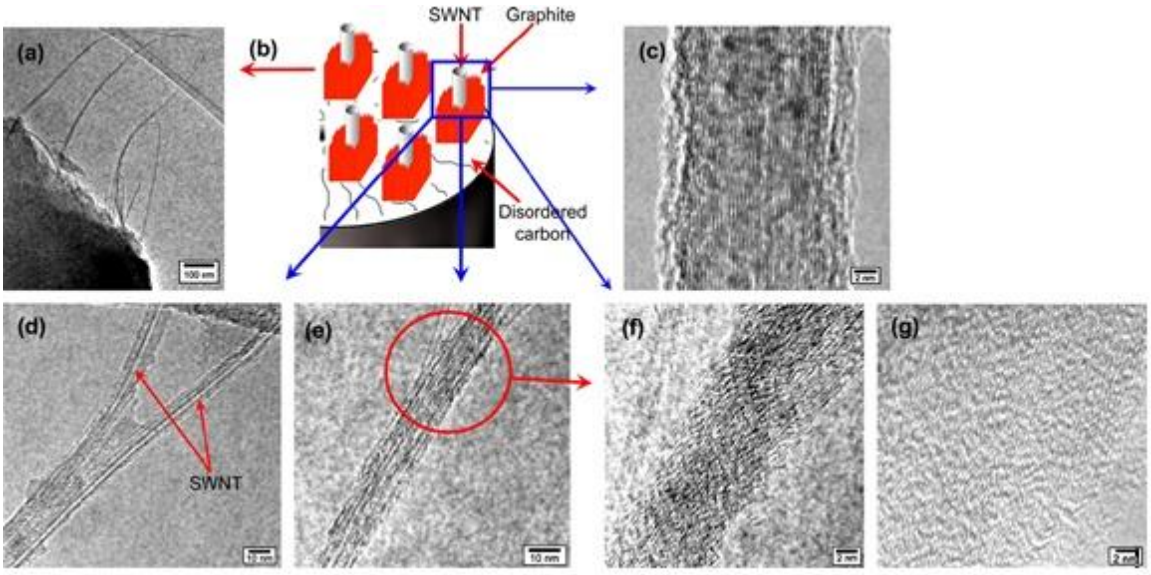

Figure 1.3 (a)-(f) TEM images and schematics of PAN/SWNT composite fiber [64]. **(g)** TEM image of control PAN [64]. Reprinted from *Polymer*, 48 (13) with permission from Elsevier.

Smaller diameter fibers have been known to result in higher strength due to a smaller probability of defects. Carbon fibers with diameters as small as 1 μm have been produced by electrospinning [65]. However, gel spinning PAN precursor polymer fibers have shown better mechanical properties when compared to other methods [66]. In order to reduce the fiber diameter, an island-in-a-sea bicomponent geometry was applied in combination with gel spinning [67] to produce PAN/CNT composite fibers and control PAN fibers. An image of the island-in-a-sea geometry is shown in Figure 1.4(a) with PMMA being the "sea" component. PMMA was removed during stabilization and the PAN/CNT composite fiber and the control PAN were carbonized at 1200°C. Figure 1.4(b) shows separated fibers where the PMMA "sea" component was dissolved by nitromethane for observation purposes. The resulting carbon fibers had an average tensile strength of 4.5 GPa and an average elastic modulus of 463 GPa [67]. However, the particular strength and modulus values were obtained from tests performed on bundles and not individual fibers.

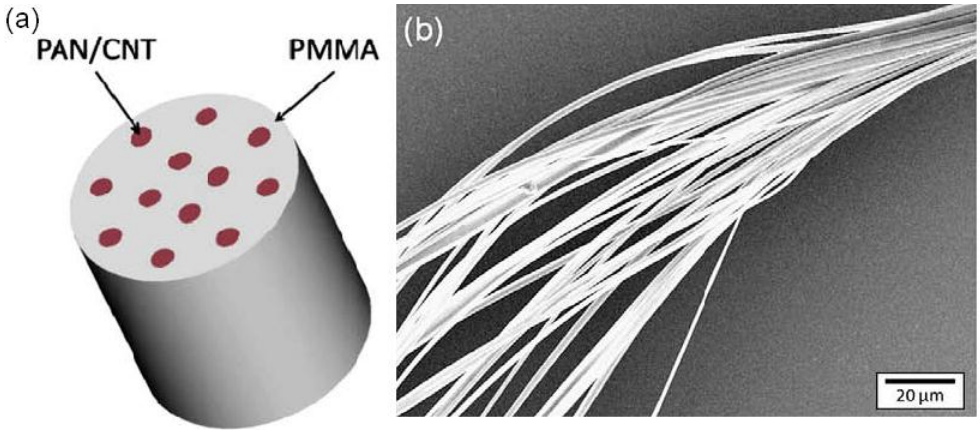

Figure 1.4 (a) Islands-in-a-sea configuration [67]. **(b)** Separated islands-in-a-sea PAN/CNT fibers [67]. Reprinted from *Composites Science and Technology*, 69 (3-4) with permission from Elsevier.

The high strength values of the composite carbon fibers have been attributed to the combination of the graphitic structure along with the load transfer ability of the nanotubes. Although processed at low temperature, 1200°C, their strength and Young's modulus compare well to the commercial fiber Torayca T-300, whose tensile strength and Young's modulus are 3.5 GPa and 230 GPa, respectively [68]. The mechanical strength, however, is a defect dependent property and commercial fibers such as the Torayca T-300 have been tested at much larger gauge lengths and were manufactured with the goal to minimize critical defects.

1.2 Objectives of this Dissertation Research

The focus of this dissertation was to measure the tensile strength of individual carbon fibers isolated from bundles, so that definitive conclusions for their properties could be drawn. Specifically, the objectives of this study were to:

- Develop the necessary methodologies to isolate and test a single carbon fibers without inducing damage
- Determine the distribution of the mechanical strength values and use statistical means to obtain the probability to attain high strength values.

Fibers were isolated from three different bundles and were placed on specially designed MEMS devices for microscale tensile testing. To fix the fiber onto a MEMS device, two different approaches were used; rigid grips made from Pt, and compliant grips made of epoxy. Digital Image Correlation (DIC) was applied to derive the stress vs. strain curves for the fibers tested. The Young's modulus was computed only from the tensile tests conducted with rigid Pt grips. The data for each bundle were analyzed by using the Weibull distribution to obtain the characteristic strength and the Weibull modulus.

CHAPTER 2

MECHANICAL PROPERTIES OF CARBON FIBERS REINFORCED WITH CNTS

PAN is the most commonly used precursor for high strength carbon fibers. In order to further increase the mechanical strength of PAN based carbon fibers, the latter have been reinforced with CNTs [67]. In this Chapter, the experiments carried out to determine the mechanical properties of CNT-reinforced PAN-based carbon fibers are described and discussed.

2.1 Materials and Specimen Preparation

Individual fibers were isolated from carbon fiber bundles derived from PAN, Figure 2.1 (a,b), with CNTs of various diameters dispersed within each individual fiber. The fibers were fabricated by the group of Professor Satish Kumar of the Material Science and Engineering Department at the Georgia Institute of Technology according to a method they developed in the past [67]. The individual fiber cross-section was not circular and was the equivalent of a circular fiber with ~1 μm diameter, as shown in Figure 2.2, where protruding CNTs can be seen. The fibers tested contained 1% wt SWCNTs and MWCNTs with respect to the precursor polymer. The CNTs were manufactured by Continental Carbon Nanotechnologies Inc., lot #X0122UA. The fibers tested were taken from 3 different bundles. Bundle #1 was received in January of 2011 and consisted of two long filaments that were ~6 cm in length. Bundles #2 and #3 were received in July of 2011. Bundle #2 was labeled as 2(412611) and was approximately 2.5

cm in length, and Bundle #3 was labeled 1(419111) and was ~5 cm in length. Large portion of each bundle was consumed to determine the best method to isolate individual carbon fibers without causing damage to the fiber gauge section.

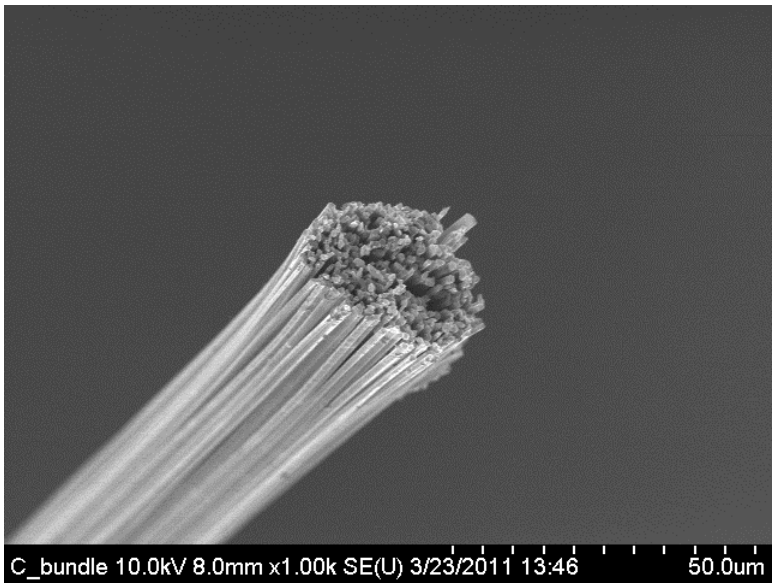

(a)

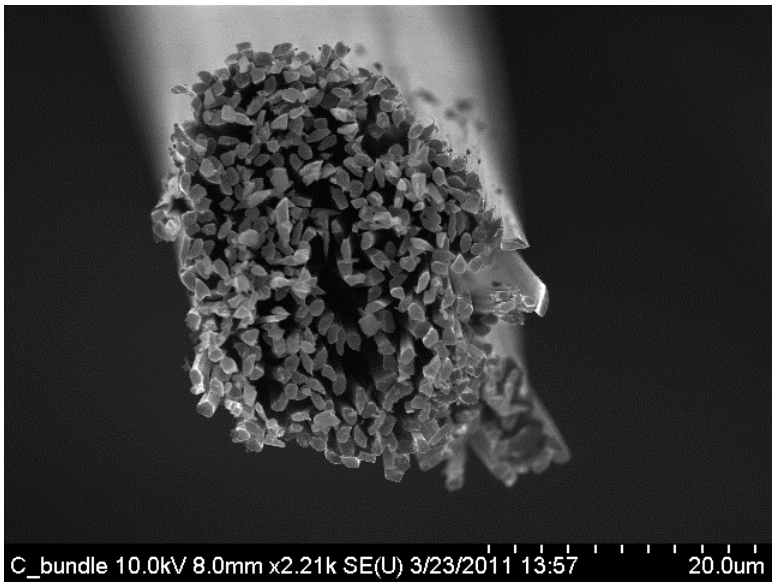

(b)

Figure 2.1 As-received bundle (bundle #1) of carbon fibers showing the cross-sections of individual fibers.

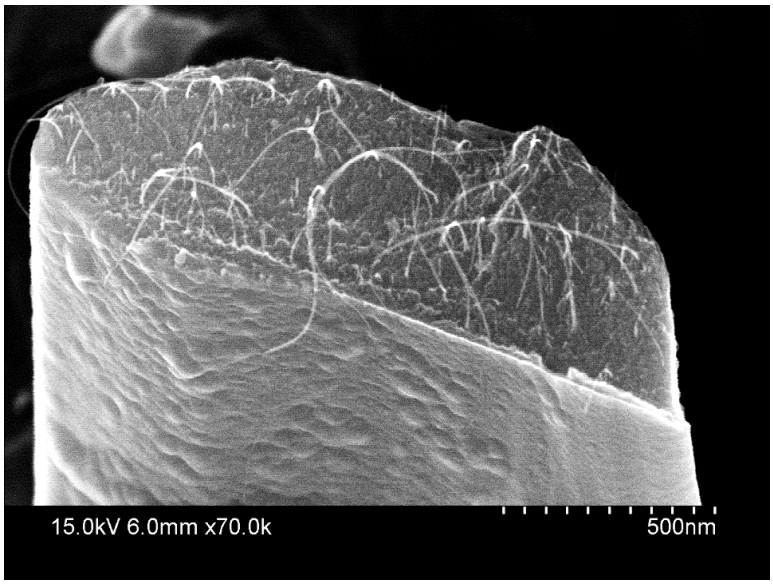

Figure 2.2 Cross-section of a tested carbon fiber showing protruding CNTs.

A total of 55 specimens were tested successfully in collaboration with Mr. Korhan Şahin. The results are presented in Chapter 3 and the order number for each experiment is presented in a cumulative manner: First experiments from bundle #1 are discussed, then experiments from bundle #3 and, finally, experiments with fibers from bundles #2 and #3 where compliant epoxy/Pt tabs were used.

Individual carbon fibers that were either 50 μm or 100 μm long were isolated for testing. This step proved challenging and a number of methods were attempted. Among the first attempts to separate fibers from a bundle involved the use of Dimethylformamide (DMF) which is effective in suspending CNTs [69,70]. The basic nature of DMF allowed for fiber dispersion [71] but it was suspected that long exposure of the carbon fibers to DMF could induce surface defects. Alternatively, the use of surfactant, dish detergent (Palmolive), in water had moderate success, but it proved impractical to pick up carbon fibers from the surfactant solution. In a different method, a piece of the fiber bundle was attached to the membrane of a speaker run at the estimated resonance frequency of the fiber bundle, at ~5.2 kHz. An input file for this purpose was created in Matlab. The tone

was played repeatedly for hours with the fiber attached to the speaker membrane using adhesive. Although the method did show moderate success, attaching and removing the fiber bundle from the speaker membrane proved to be impractical.

In an alternate approach, a piece of carbon fiber bundle of a few millimeters in length was cut from the main bundle using an exact-o knife attached to a probe stage. When cut, the fiber ends were somewhat frayed which made possible to pull fibers from the bundle using the frayed end. This approach was precise and ensured that the fiber was only handled by its ends while the gauge section remained pristine. Originally, this process was applied in water as the cut fiber broke away. After multiple iterations, however, it became possible to carry out this process in air, as shown in Figure 2.3.

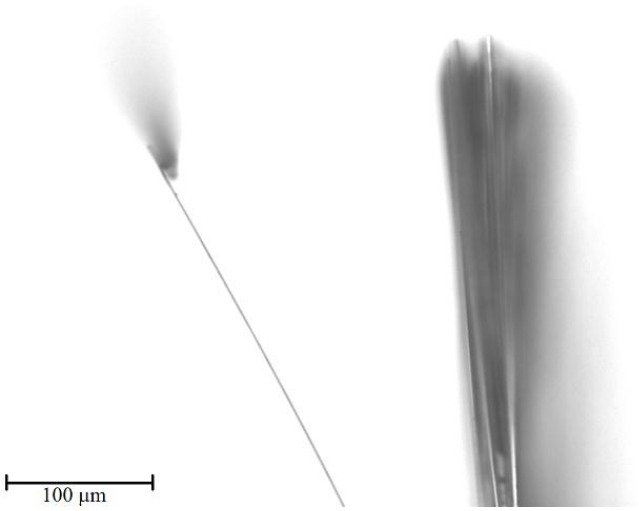

Figure 2.3 Single fiber pulled from a bundle by a tungsten probe.

2.2 MEMS Devices for Microscale Carbon Fiber Testing

MEMS devices for nanofiber testing were employed due to the small size of the carbon fibers (1 μm in diameter and 50-100 μm in length). The devices were designed by Mr. Korhan Şahin and Mr. David Grossman of Professor Chasiotis' research group and were fabricated at Sandia National Laboratories in Albuquerque, NM. The device design

was based on previous works by this group [72-76]. A 3×4 mm^2 chip contained MEMS devices with loadcells of 3 nominal stiffnesses: 500 N/m, 2,000 N/m and 4,000 N/m. Most of the experiments were run using the 500 N/m devices, which were calibrated by Mr. Korhan Şahin to have an actual stiffness of 322 N/m. A close up image of a 500 N/m stiff device is shown in Figure 2.4. Devices of 2,000 N/m stiffness with some of the loadcell beams cut, as shown in Figure 2.5, were used due to shortage of the lower stiffness devices. The 2,000 N/m stiff MEMS devices, reduced to half the nominal stiffness (1,000 N/m), were calibrated to have an actual stiffness of 447 N/m. Due to concern that a very strong fibers could break the lowest stiffness MEMS devices, 2,000 N/m stiff MEMS devices with half of their loadcell beams cut were preferable.

The basic components of the aforementioned MEMS devices are labeled in Figure 2.4(a). Sections labeled I and II are the fixed and the moving grip, respectively, with the fiber being firmly mounted between the two sections. Section III is a folded beam loadcell comprised of two components separated in the middle of the section and attached by parallel beams on each side. The device shown in Figure 2.4(a,b) has 500 N/m stiffness. Higher stiffness devices have more beams and/or larger thickness. The beams deflect as the fiber is loaded so that the two components of section III move apart. The right hand portion of section III is fixed to an external glass probe attached to the pedal in section V, as shown later in Figure 2.9. The movement in the left hand side of Section III is due solely to the load applied on the fiber. The 3 staples shown in Section IV ensured that the fiber in Section I was subjected to a purely axial load resulting in tensile stresses in the fiber. Finally, the 4 tethers shown in Section V are used to keep the device suspended and are broken before testing.

The carbon fibers were held in place on the device by an optical adhesive cured by UV light. The adhesive was placed on the device at both ends of the fiber in very small amounts using a probe with ~1 μm diameter tip. The carbon fiber was then placed in the adhesive and was left to cure. In later experiments, a layer of adhesive was first applied to the surface and cured. More adhesive was then applied on top of the cured

layer, and the carbon fiber was then placed. This process prevented direct contact of the carbon fiber with the potentially abrasive surface of the polysilicon MEMS device.

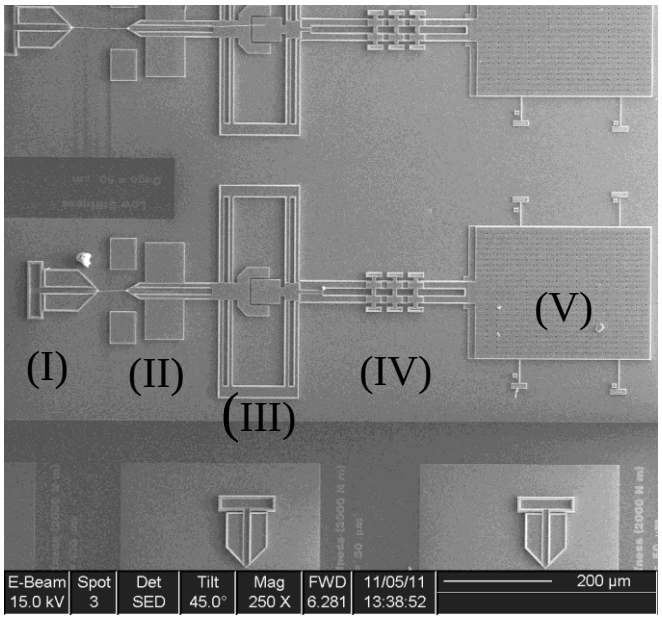

(a)

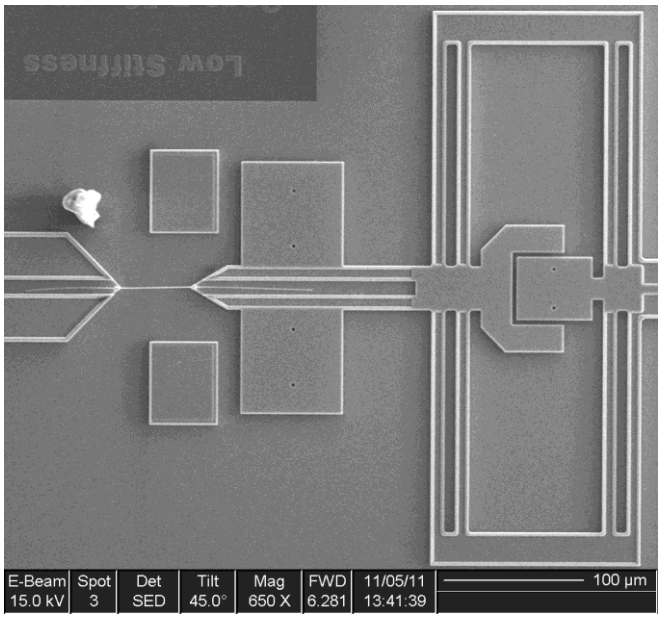

(b)

Figure 2.4 (a) Low stiffness MEMS device showing the individual components: (I) stationary grip, (II) moving grip, (III) load cell, (IV) staples, (V) pedal **(b)** Detail of load cell and mounted carbon fiber. SEM images were acquired by Mr. Korhan Şahin.

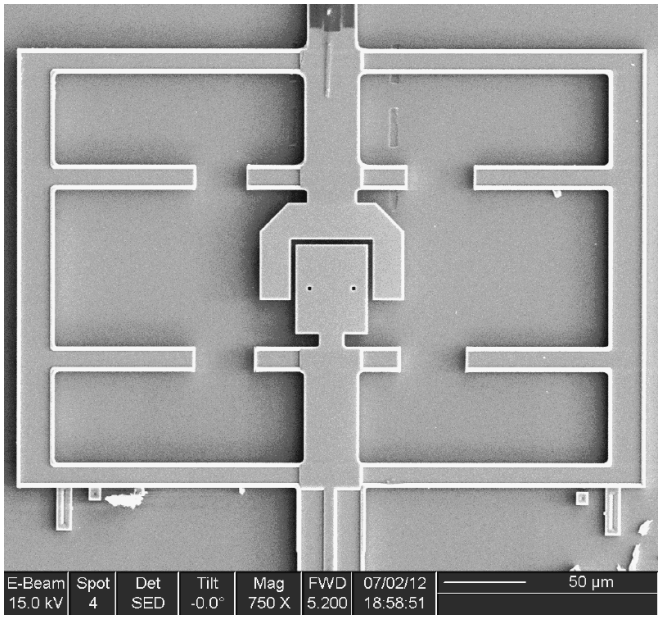

Figure 2.5 Medium stiffness device with cut beams to reduce its stiffness. Image was taken after an experiment was completed.

The UV adhesive was strong enough to keep the fiber temporarily in place, but it would yield during a tension experiment. For this reason, the FEI Dual Beam 235 FIB located in the Materials Research Lab at UIUC was used to deposit platinum (Pt) tabs on both ends of the fiber via the ion beam. This process was done in two steps to ensure full coverage. First, Pt was deposited on either side of the carbon fiber with small overlap as shown in Figure 2.6(a). The height of the two depositions was approximately 0.5 µm. Next, a Pt bridge was deposited on the fiber as shown in Figure 2.6(b). The height of Pt deposited on the bridge was 0.75-1 µm depending on the fiber diameter. The ion beam was used to deposit Pt at a current of 50 pA. The low current prolonged the mounting process but also minimized damage to the fiber due to the ion beam. Care was taken to ensure that the gauge section of the carbon fiber was not exposed to the ion beam during patterning. If properly done, the grips were strong enough to hold the fiber in place during a tension test.

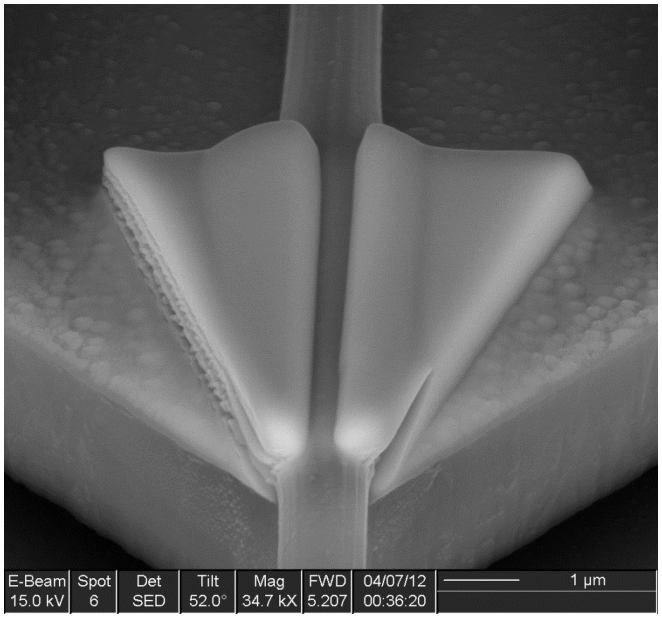

(a)

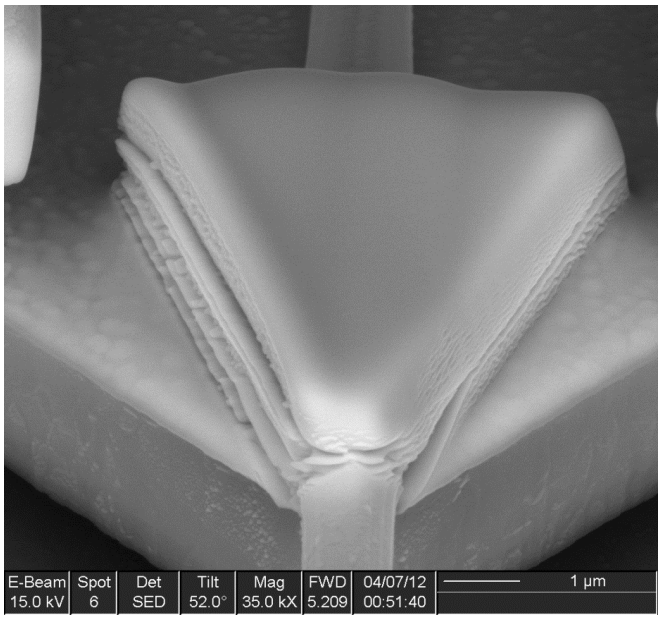

(b)

Figure 2.6 (a) Initial 0.5 µm deposition to ensure full coverage of Pt around the fiber, **(b)** bridge to fix the fiber onto the MEMS device.

Despite the fact that no damage was visible on the carbon fibers fixed with the aid of Pt tabs, there was reason to believe the ion beam could still cause damage to the fiber. As the fiber ruptured at the end of each experiment, it shattered and the fragments flew away. In order to collect the broken pieces, tests were carried out in glycerin. These experiments revealed that in most cases the fibers probably broke at the Pt tabs. Furthermore, SEM images, e.g. see later Figure 3.11, showed that deposition of Pt created a very thin amorphous region on the outer layer of the carbon fiber near the grip region, which opens the possibility for ion beam induced defects near the grips, which would compromise the fiber strength. However, no visible signs of fiber damage were detected in SEM images near the Pt tabs. In order to elucidate this potential issue, experiments were carried out by gripping the fibers using an epoxy. The latter is inherently compliant and, therefore, does not allow for accurate calculation of the fiber's Young's modulus. However, the strength values yielded from these experiments eliminate concerns arising from Pt damage at the grips.

Bonding only via an epoxy adhesive is not strong enough and the fiber eventually pulled out from the grips. To address this problem, a combination of epoxy and Pt was applied which resolved this problem. Pt was deposited far away from the point of fiber attachment to the grips. Additionally, Pt patches of 1-μm thickness were deposited on the surface of the fiber and sufficiently far away from the tip of the grips. Because of the use of the compliant epoxy adhesive at the tip of the grips, the clamping force on the fiber during axial loading was reduced. Furthermore, as the interfacial shear stress between the fiber and the epoxy decreased away from the tip of the grips, the Pt tabs shared part of the force transmitted from the grip to the fiber serving as mechanical slip locks. The arrangement of the Pt tabs is shown in Figure 2.7(a-b). Once the Pt tabs were deposited, the entire fiber on the grips was covered with epoxy.

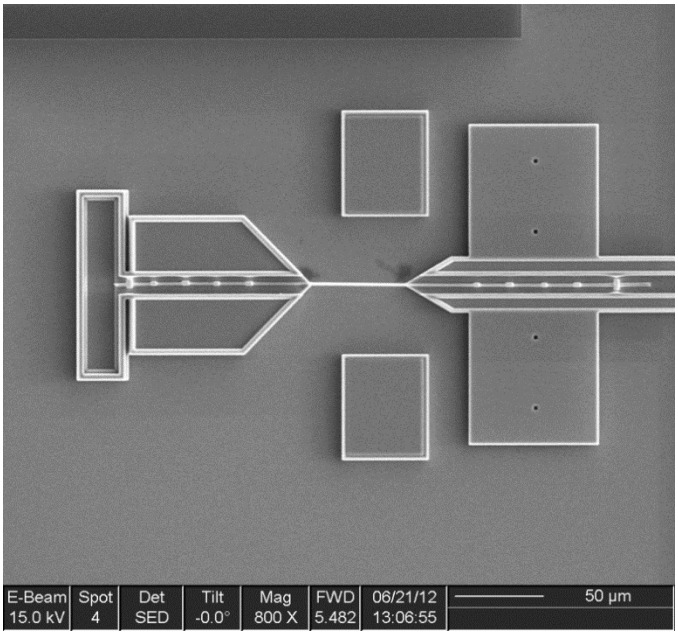

(a)

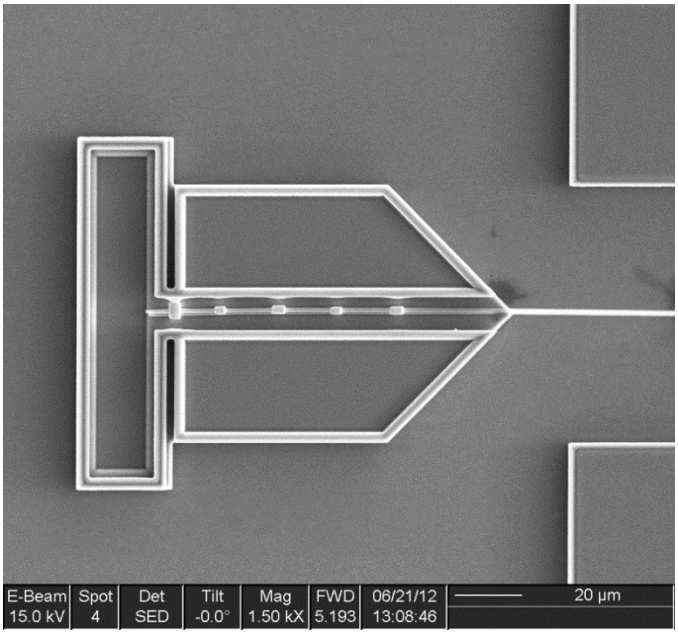

(b)

Figure 2.7 (a) Pt tabs deposited far away from the gauge section on the fixed and moving grips, **(b)** close up of fixed grip.

2.3 Experimental Procedures

MEMS chips with mounted carbon fibers were placed onto the experimental apparatus shown in Figure 2.8. A piezoelectric actuator provided motion to the on-chip testing device and the requisite force and actuation range. A flat glass probe was used to connect the external piezoelectric actuator with the MEMS loadcell. The glass probe was cut out of a glass slide and was mounted using a UV curable adhesive. The glass probe was gently placed onto the pedal, Figure 2.9, using a linear stage and micrometer driven x-y stage and the adhesive was allowed to cure. A digital camera recorded the MEMS device motion at 15 fps. Dark field optical imaging was used to produce a fine speckle pattern on device, which is shown in the boxes in Figure 2.10. This fine random speckle pattern was necessary so that Digital Image Correlation (DIC) could be used effectively to calculate the device motion with an accuracy of ~25 nm [77].

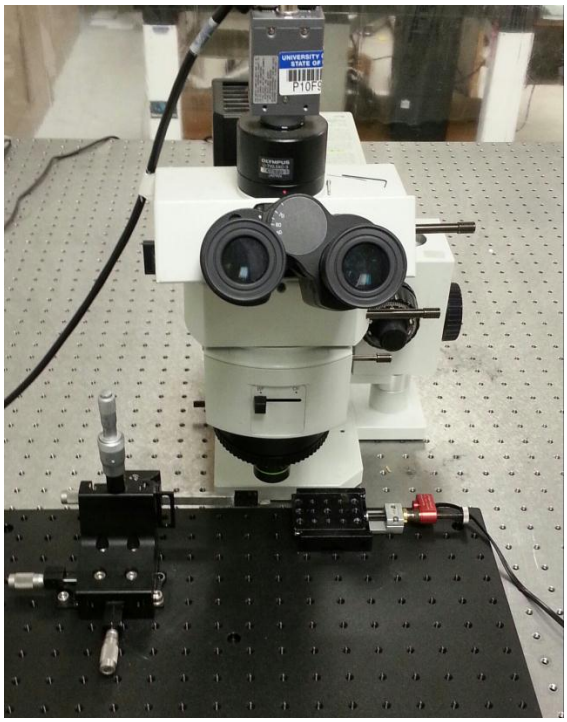

Figure 2.8 Experimental set up.

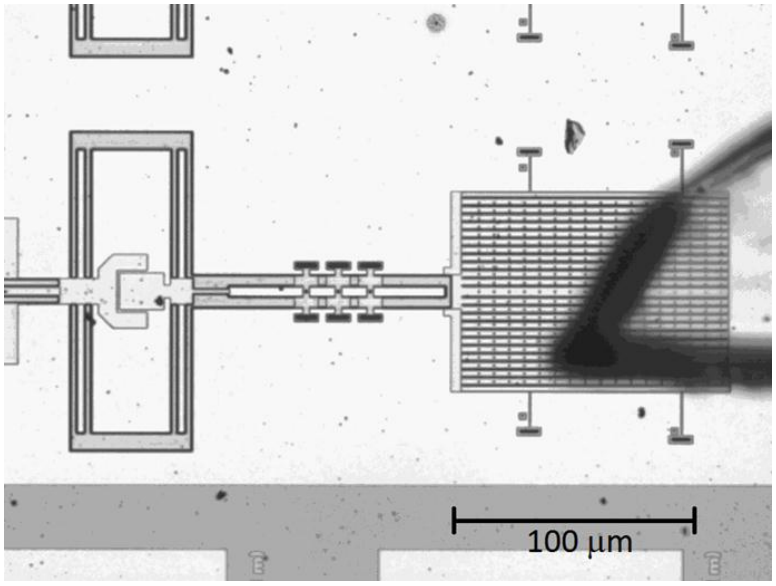

Figure 2.9 Glass probe placed onto the MEMS device pedal.

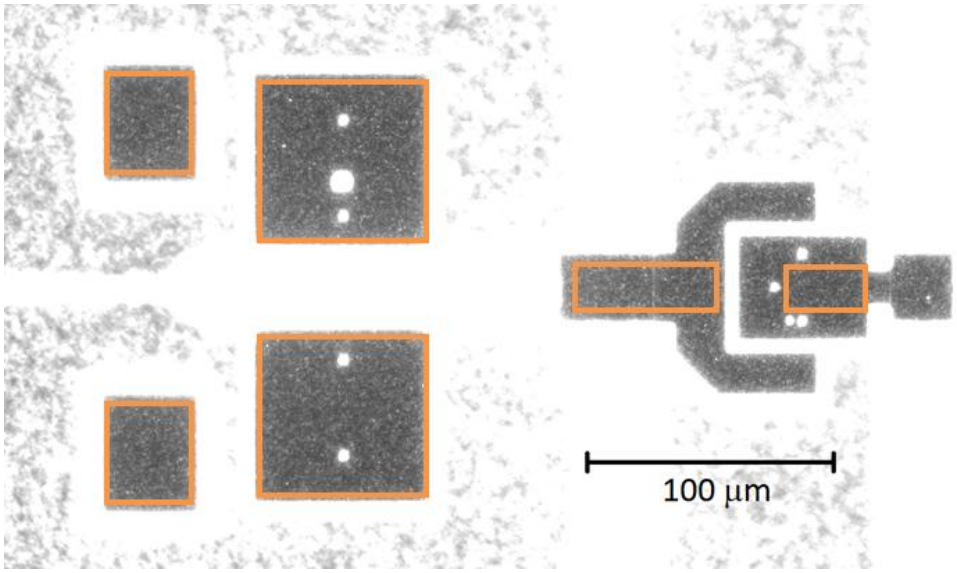

Figure 2.10 Fine speckle pattern generated by dark field optical imaging to facilitate the application of DIC.

2.4 Post-experimental Analysis

DIC (VIC-2D 2009) was applied to extract a stress vs. strain curve for each fiber. The strain in a fiber was calculated from the displacement between the two red boxes labeled "A" in Figure 2.11. The difference in the motion of the device and the movement due to the load cell opening is equal to the elongation of the carbon fiber. Since the length of the fiber gauge section was known, strain could be calculated. Similarly, the stress could be calculated from the motion of the two regions labeled "B" in Figure 2.11. The blue box on the left moved with the opening of the load cell, and the blue box on the right was stationary due to the glass probe attached to the pedal. Therefore, the difference in the motion of these two regions provided the opening of the load cell. The stiffness of the load cell was determined by direct calibration. The product of the loadcell opening with its stiffness provided the force applied to the carbon fiber. The stress was then calculated by dividing the applied force by the fiber's measured cross-sectional area.

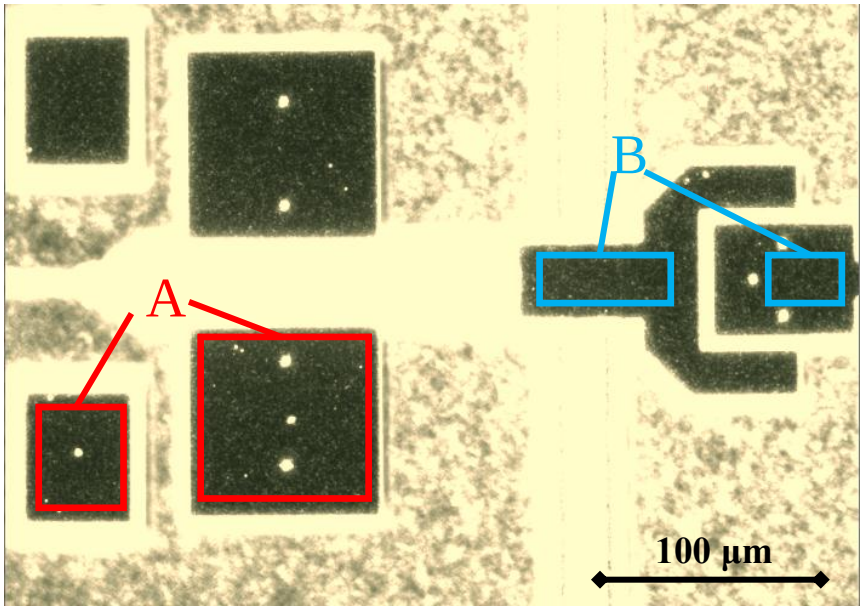

Figure 2.11 Correlation areas used in the calculation of the motion of the device components by DIC.

DIC is a full-field displacement/strain measurement method, which, in this work was used to compute the in-plane rigid body motions by comparing surface patterns on components of the MEMS during fiber loading [72-76]. Large subset sizes are generally desirable as they provide "smoothing" of the displacement field which is acceptable in the absence of displacement gradients. The speckle pattern generated on the surface of MEMS devices using dark field imaging have been shown by this group to provide displacement resolution on the order of 25 nm [77].

2.5 Conclusions

In this Chapter, the experimental methods for isolating and testing individual carbon fibers isolated from bundles were discussed. Due to their minute size, the fibers were tested with specially designed MEMS devices. Two methods were used to assure a robust fiber attachment. The first used Pt tabs deposited by a FIB. The second method employed a polymer adhesive in conjunction with Pt mechanical locks. The use of Pt tabs guaranteed the correct measurement of the elastic modulus of the carbon fibers, while the use of combined Pt/epoxy tabs reduced the risk of fiber failure at the grips. Results from each gripping method are described in Chapter 3. Measurements of the applied force and the fiber extension were carried out with the use of DIC which guaranteed independent and high resolution data for each quantity.

CHAPTER 3

STATISTICAL DESCRIPTION OF FIBER STRENGTH

Mechanical property experiments were run with single carbon fibers to determine their tensile strength and elastic modulus. Due to their brittle nature, there is no unique value for their mechanical strength and, therefore, the failure strength data must be analyzed in terms of probability of survival, or failure, at a given stress. The statistical distribution function that accurately describes the failure of brittle materials has been developed by Waloddi Weibull in 1939 [78] and was applied to the results of this research.

3.1 Weibull Statistics Applied to Mechanical Strength Data

In the Weibull probability density function the survival probability of a specimen, $P_s(\sigma, V_0)$, is defined as the fraction of samples with volume, V_0, that survive a uniform stress, σ. Specifically, $P_s(V_0)$ is given by,

$$P_s(\sigma, V_0) = \exp\left[-\left(\frac{\sigma}{\sigma_0}\right)^m\right] \quad (1)$$

where σ_0 and m are "material" constants. It is clear from this equation that $P_s(\sigma, V_0)$ =1 when σ=0, meaning that no samples will fail. The parameter m is the Weibull modulus: a lower value of m indicates higher variability in tensile strength of a component [79]. If $\sigma=\sigma_0$, it can be easily seen from Equation (1) that $P_s(\sigma, V_0)$ = 1/e, which is ~0.37. Thus, σ_0, the Weibull characteristic strength, is the stress at which 37% of the samples will survive.

The values of σ_0 and m are determined using experimental data along with Equation (1). The strength of each sample with volume V_0 is plotted against a probability estimator function to determine the percentage of survival. The probability estimator function used for the present experimental data was:

$$P_j = (j - 0.5)/n \tag{2}$$

Here n and j are defined by ordering the strength values as $\sigma_1 \leq \sigma_2 \leq \ldots \leq \sigma_j \leq \ldots \leq \sigma_n$. The probability estimator in Equation (2) was chosen because it gives the most accurate results when the sample size $n \geq 20$ [80]. The value of m is determined from the following form of Equation (1):

$$\ln\left[\frac{1}{P_s(\sigma, V_0)}\right] = \left(\frac{\sigma}{\sigma_0}\right)^m \tag{3}$$

or the more convenient expression:

$$\ln\left\{\ln\left[\frac{1}{P_s(\sigma, V_0)}\right]\right\} = m\ln\left(\frac{\sigma}{\sigma_0}\right) \tag{4}$$

Equations (1), (3), (4) are valid for specimens that have the same volume. The fibers tested in this work had different cross-sections and gauge lengths 50 or 100 μm. Therefore, Equation (1) must be written to account for volume variations:

$$P_s(\sigma, V) = \exp\left[-\frac{V}{V_0}\left(\frac{\sigma}{\sigma_0}\right)^m\right] \tag{5}$$

where V is the volume of a specimen and V_0 is a reference volume. The volume of a given specimen can be defined by some multiple, k, of the reference volume; $V = kV_0$. Thus, Equation (5) can be rewritten as

$$P_s(\sigma, V) = \exp\left[-k\left(\frac{\sigma}{\sigma_0}\right)^m\right] \tag{6}$$

From this expression, k and σ can be combined to form a reduced stress that takes the specimen volume into account [81] and is defined as

$$s = \sigma k^{1/m} \tag{7}$$

Putting Equation (6) in terms of the reduced strength we obtain

$$P_s(\sigma, V) = \exp\left[-\left(\frac{s}{\sigma_0}\right)^m\right]. \tag{8}$$

Equation (8) makes use of stress values that have been corrected for the volume of each specimen and yields a more consistent and "the true" value of m. Similarly to Equations (1) and (4), the volume corrected Equation (8) can be written as:

$$\ln\left\{\ln\left[\frac{1}{P_s(\sigma, V)}\right]\right\} = m\ln\left(\frac{s}{\sigma_0}\right), \tag{9}$$

in order to calculate easily the Weibull modulus.

It should be noted that the *three* parameter Weibull probability density function is often used:

$$P_s(\sigma, V_0) = \exp\left[-\frac{V}{V_0}\left(\frac{\sigma-\sigma_u}{\sigma_0}\right)^m\right], \tag{10}$$

where σ_u is a threshold stress at which the probability of failure is zero and is taken as equal to zero in all previous equations. When σ_u=0, P_s in Equation (10) is equal to *one* only when σ=0, thus, yielding a conservative estimation. However, since it is very difficult to guarantee a minimum strength value for brittle materials, it is often recommended that σ_u is taken as *zero* [82].

3.2 Calculation of Weibull Parameters for Individual Carbon Fibers

The Weibull probability density function was used to statistically describe the tensile strength results obtained in this study. The results from experiments conducted on fibers from bundle #1 are listed in Table 3.1. In the first column, the strength data are ordered in increasing value without accounting for variations in the specimen volume. Calculations that used the strength data in this column resulted in m = 4.16. If Equation (9) is applied it emerges that the order of the newly calculated "volume corrected strength" data is not in ascending any longer, as verified by the last column in Table 3.1. The Weibull analysis was then run again using the values of measured strength ordered according to the ascending order of the data in the last column of Table 3.1. The entire analysis was repeated, and the true value of m was found to be equal to 4.4 using the graph in Figure 3.1, while σ_0 was found to be equal to 4.13 GPa according to Equation (9). The volume corrected analysis was carried out with respect to a reference fiber with 1 μm effective diameter and 50 μm gauge section.

Given the calculated Weibull probability density function values, the volume corrected reduced strength was obtained from Equation (7). Table 3.2 presents the strength values in the correct order after accounting for the fiber volume, and the resulting volume corrected reduced strength. In Figure 3.2, the probability estimator function calculated by Equation (2) is plotted against the reduced strength values, shown as the blue discrete points. The probability function from Equation (8) is then fitted against the data points, showing excellent agreement. A close fit is expected, since the results of Equation (8) are a function of m and σ_0 which are output by the probability estimator function in Equation (2). The fact that the data closely follow a Weibull plot and the probability function calculated with Equation (8) is in good agreement support the validity of the present analysis and the use of an appropriate probability estimator for the given sample size.

SEM images of the cross-sections of fibers from bundle #1 showed various shapes categorized as elliptical, rectangular and irregular. Specifically, nine fibers with elliptical

cross-section from bundle #1 had average strength of 3.65±1.07 GPa, three fibers with approximately rectangular cross-section had average strength of 2.99±0.51 GPa, and nine fibers with irregular cross-section, had average strength of 3.30 ± 0.96 GPa. Examples of fibers with elliptical, rectangular and irregular cross-sections are provided in Figures 3.3(a-c), Figure 3.4(a-c) and Figure 3.5(a-c), respectively. Given the limited number of samples, it is difficult to draw general conclusions. However, it appears that fibers with elliptical cross-sections resulted in the highest average strength due to the lack of ridges, corners, cusps and other forms of stress concentrations.

Table 3.1 Experimental strength data from bundle #1 ordered according to the measured values of tensile strength.

Strength (σ) (GPa)	**Young's Modulus (GPa)**	**Gauge Length (μm)**	**Effective Diameter (μm)**	**$\ln((V/V_0)^{1/m}*\sigma)$**
1.91	159	50	0.82	**0.56**
2.16	184	50	1.22	**0.86**
2.54	223	50	1	**0.93**
2.65	209	100	1	**1.13**
2.86	167	50	1.07	**1.085**
2.88	264	50	1.6	**1.27**
3.16	237	50	1.36	**1.29**
3.25	247	100	0.95	**1.31**
3.31	261	100	1.09	**1.39**
3.36	131	50	1	**1.21**
3.43	231	50	0.81	**1.14**
3.54	260	100	1.08	**1.46**
3.55	259	100	1	**1.42**
3.76	220	100	0.99	**1.48**
3.97	170	50	0.99	**1.37**
4.03	269	100	0.85	**1.48**
4.31	240	100	0.97	**1.60**
4.47	289	50	0.96	**1.48**
4.88	232	50	0.98	**1.58**
5.66	300	50	1.03	**1.75**

Table 3.2 Experimental strength values ordered after volume correction and reduced strength values for fibers from bundle #1.

Strength (GPa)	Gauge Length (μm)	Effective Diameter (μm)	$\ln((V/V_0)^{1/m}*\sigma)$	Reduced Strength (GPa)
1.91	50	0.82	0.56	**1.75**
2.16	50	1.22	0.86	**2.36**
2.54	50	1	0.93	**2.54**
2.86	50	1.07	1.08	**2.95**
3.43	50	0.81	1.14	**3.12**
2.65	100	1	1.13	**3.10**
3.36	50	1	1.21	**3.36**
2.88	50	1.6	1.27	**3.57**
3.16	50	1.36	1.29	**3.63**
3.25	100	0.95	1.31	**3.72**
3.97	50	0.99	1.37	**3.95**
3.31	100	1.09	1.39	**4.03**
3.55	100	1	1.42	**4.16**
3.54	100	1.08	1.46	**4.29**
4.47	50	0.96	1.48	**4.39**
4.03	100	0.85	1.48	**4.38**
3.76	100	0.99	1.48	**4.38**
4.88	50	0.98	1.58	**4.84**
4.31	100	0.97	1.60	**4.98**
5.66	50	1.03	1.75	**5.74**

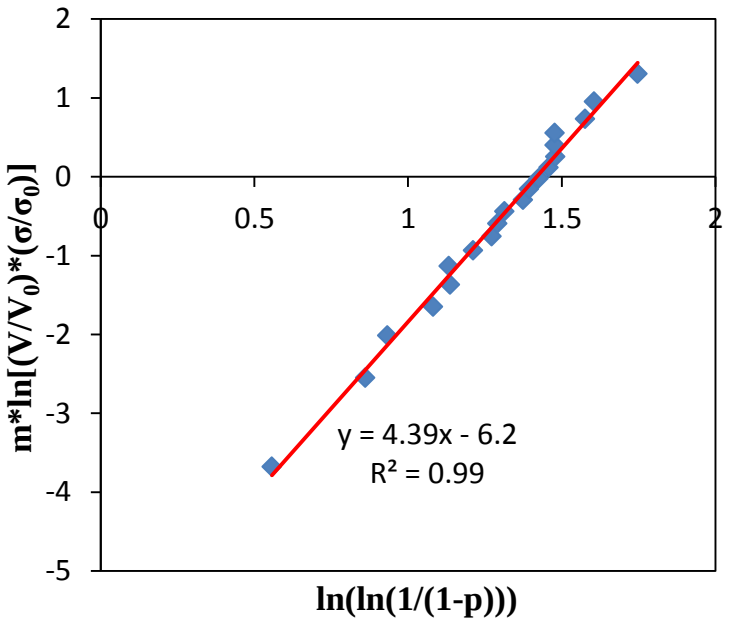

Figure 3.1 Equation (9) plotted for the data from bundle #1.

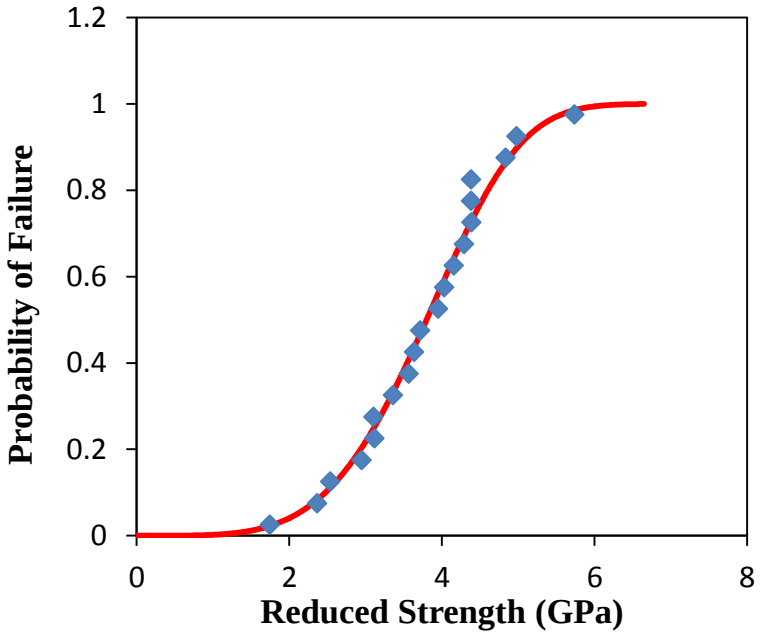

Figure 3.2 Weibull probability function (red curve) plotted with reduced strength values (blue points) for data from bundle #1.

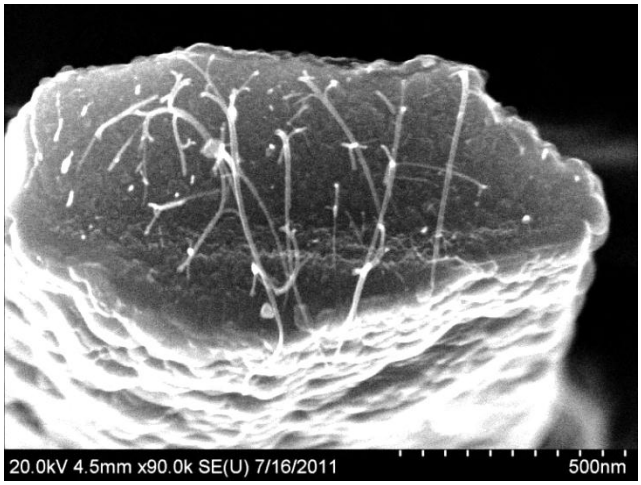

(a)

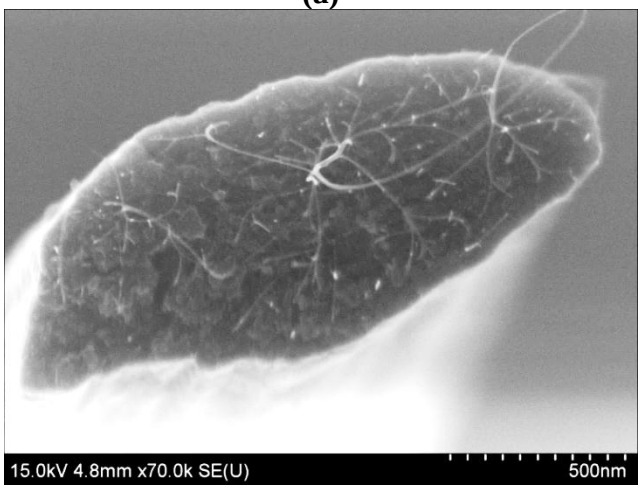

(b)

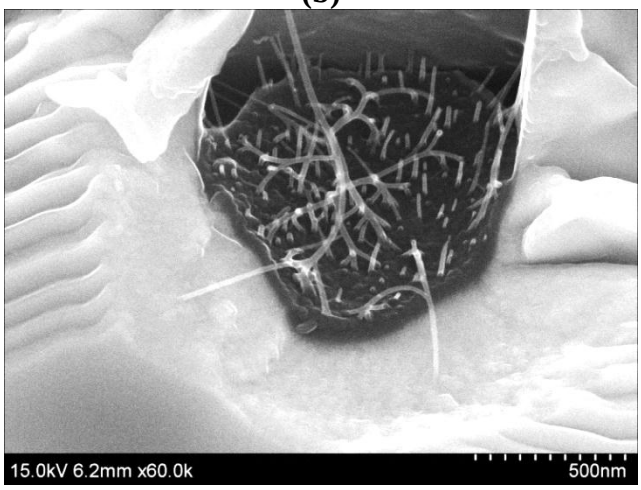

(c)

Figure 3.3 Fibers with elliptical cross-sections from bundle #1 and experiments **(a)** #9, **(b)** #13, and **(c)** #4. SEM images were acquired by Mr. Korhan Şahin.

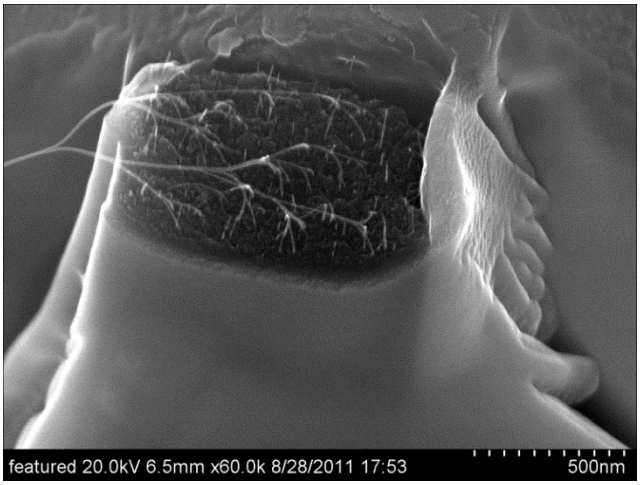

(a)

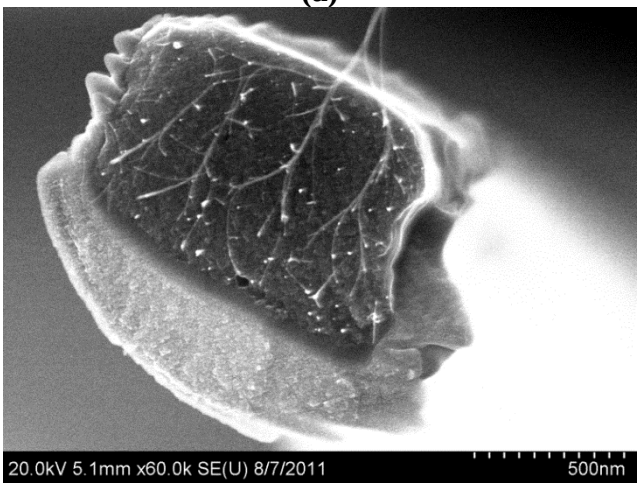

(b)

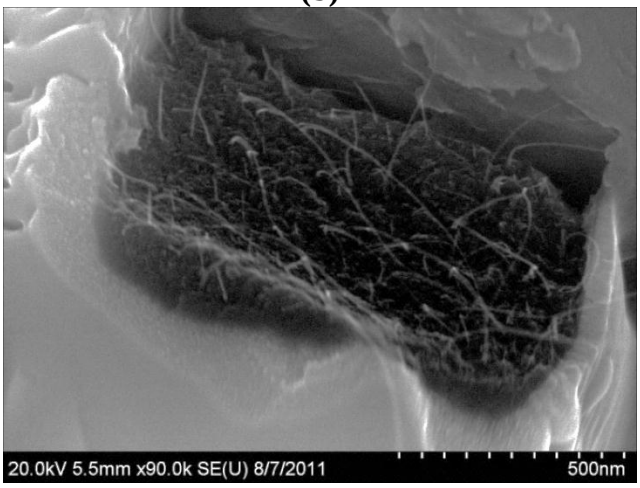

(c)

Figure 3.4 Fibers with rectangular cross sections from bundle #1 and experiments **(a)** #19, **(b)** #15, and **(c)** #16. SEM images were acquired by Mr. Korhan Şahin.

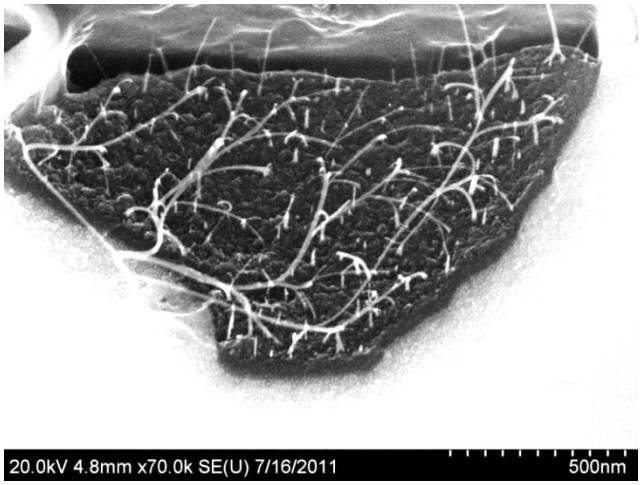

(a)

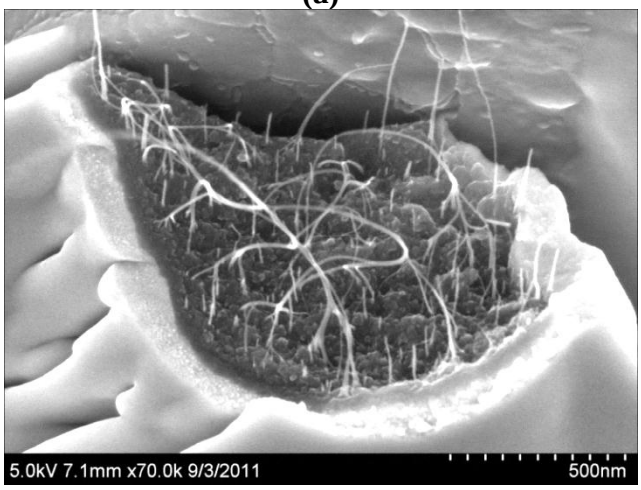

(b)

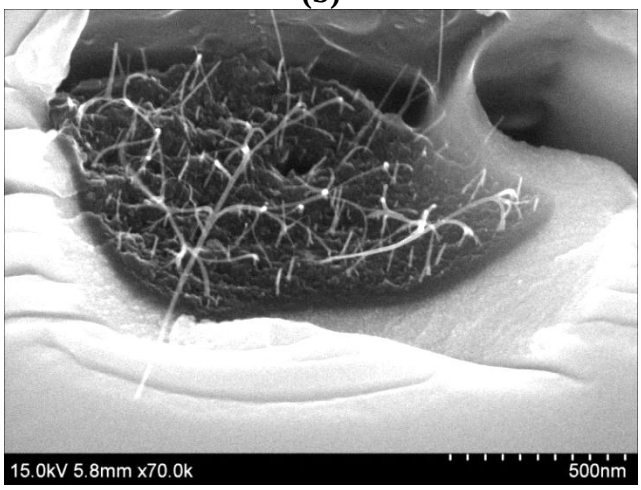

(c)

Figure 3.5 Fibers with irregular cross-sections from bundle #1 and experiments **(a)** #8, **(b)** #21, and **(c)** #5. SEM images were acquired by Mr. Korhan Şahin.

The experimental data from bundle #3 were analyzed in a similar manner as those from bundle #1. The data were initially ordered according to measured strength values, as shown in the first column of Table 3.3. After fitting an initial m=3.97, the data were reordered in ascending order following Equation (9), and are listed in the rightmost column of Table 3.3. The strength data of the first column of Table 3.3 were re-ordered with a correction for specimen volume according to the ascending order of the values in the last column in Table 3.3, and this new order is given in the first column on Table 3.4. The volume corrected analysis was done with respect to a reference fiber with 1 μm effective diameter and 50 μm gauge section. The analysis was repeated to compute m=4.13, as shown in Figure 3.6, and σ_0 =5.07 GPa by using Equation (9). The volume corrected reduced strength values calculated by Equation (7) are given in the right-most column of Table 3.4. The probability estimator function from Equation (2) is plotted against reduced strength data and is shown as the blue discrete points in Figure 3.7. The probability function from Equation (8) is also plotted in red in Figure 3.7 and is in good agreement with the discrete data points. As discussed for the case of bundle #1, the close fit and the good Weibull trend indicate a good choice for the probability estimator, and the appropriateness of the aforementioned procedure for statistical analysis.

Similarly to bundle #1, SEM images of the failure cross-sections of fibers from bundle #3 were obtained. They were also categorized as elliptical, rectangular, and irregular. Examples of such cross-sections are shown in Figure 3.8(a-c), Figure 3.9(a-c) and Figure 3.10(a-c), respectively. Ten fibers with elliptical cross-sections had average tensile strength of 4.23±1.26 GPa, three fibers with rectangular cross-section had average strength of 4.14±1.53 GPa, and twelve fibers with irregular cross-section had average strength of 4.92±1.46 GPa. Similarly, to bundle #1, carbon fibers with rectangular cross-sections had the lowest tensile strength, although not significantly lower than fibers with elliptical cross-sections. In bundle #3 fibers with irregular cross-section had the highest strength. However, given the close average strength values for the 3 cross-sectional geometries, it appears that none of them can be definitively associated with a higher probability for high strength.

Table 3.3 Experimental strength data from bundle #3 ordered according to the measured values of tensile strength.

Strength (σ)	Young's Modulus (GPa)	Gauge Length (μm)	Effective Diameter (μm)	$\ln((V/V_0)^{1/m}*\sigma)$
1.87	227	100	0.9	0.75
2.45	192	100	0.99	1.07
2.92	294	100	0.68	1.05
3.28	226	50	0.94	1.16
3.36	251	50	0.95	1.19
3.41	272	100	0.83	1.31
3.48	263	50	0.85	1.17
3.48	298	100	0.95	1.40
3.63	254	100	0.96	1.44
3.96	284	100	0.94	1.52
4.32	266	50	0.88	1.40
4.5	229	50	0.94	1.47
4.5	264	100	1.02	1.69
4.58	207	50	0.99	1.52
4.78	179	50	1.05	1.59
4.97	256	50	0.99	1.60
5.16	247	50	0.79	1.52
5.19	289	100	0.8	1.71
5.82	212	50	1	1.761
5.83	298	50	1	1.761
5.86	224	50	0.88	1.701
6.05	303	100	0.88	1.911
6.21	234	50	0.93	1.79
6.88	248	50	0.91	1.88
7.24	323	50	0.96	1.96

Table 3.4 Experimental strength values ordered after volume correction and reduced strength values for fibers from bundle #3.

Strength (GPa)	Gauge Length (μm)	Effective Diameter (μm)	$\ln((V/V_0)^{1/m}*\sigma)$	Reduced Strength (GPa)
1.87	100	0.9	0.74	2.10
2.92	100	0.68	1.05	2.87
2.45	100	0.99	1.06	2.88
3.28	50	0.94	1.16	3.18
3.48	50	0.85	1.17	3.22
3.36	50	0.95	1.19	3.28
3.41	100	0.83	1.30	3.68
3.48	100	0.95	1.39	4.01
4.32	50	0.88	1.40	4.06
3.63	100	0.96	1.437	4.21
4.5	50	0.94	1.47	4.37
3.96	100	0.94	1.51	4.54
4.58	50	0.99	1.52	4.56
5.16	50	0.79	1.53	4.60
4.78	50	1.05	1.59	4.89
4.97	50	0.99	1.60	4.95
4.5	100	1.02	1.68	5.37
5.19	100	0.8	1.71	5.51
5.86	50	0.88	1.71	5.51
5.82	50	1	1.76	5.82
5.83	50	1	1.76	5.83
6.21	50	0.93	1.79	6.00
6.88	50	0.91	1.88	6.57
6.05	100	0.88	1.91	6.73
7.24	50	0.96	1.96	7.10

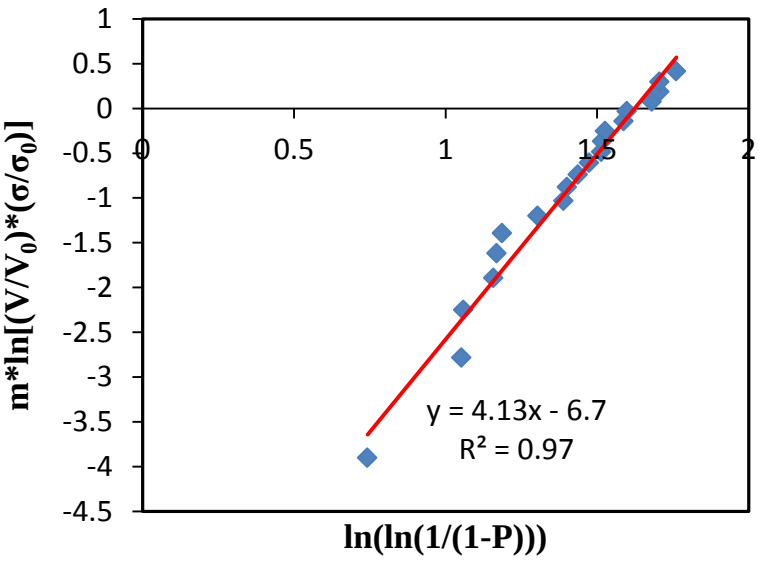

Figure 3.6 Equation (9) plotted for the data from bundle #3 to obtain the Weibull modulus.

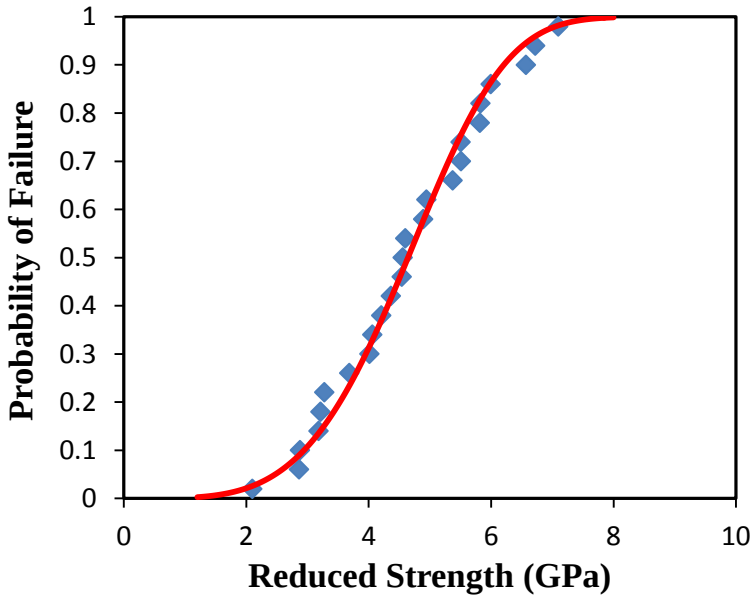

Figure 3.7 Weibull probability function (red curve) plotted against the reduced strength values (blue points) for fibers from bundle #3.

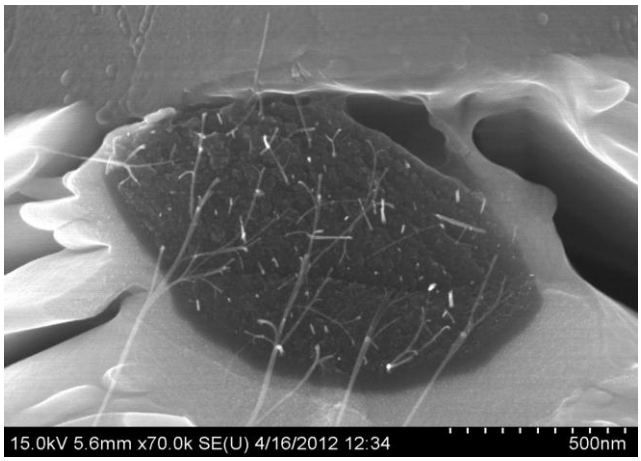

(a)

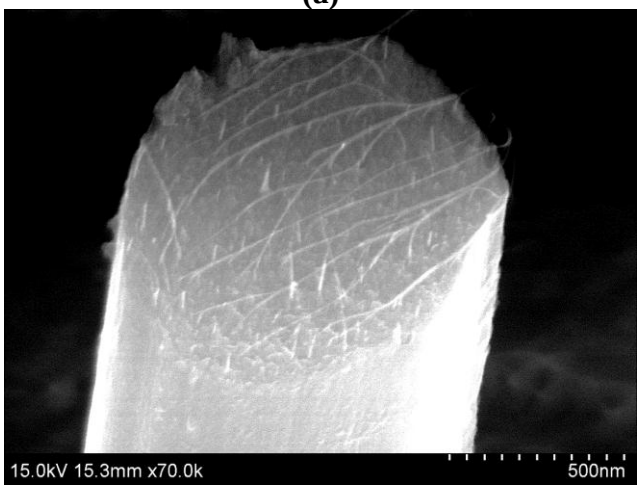

(b)

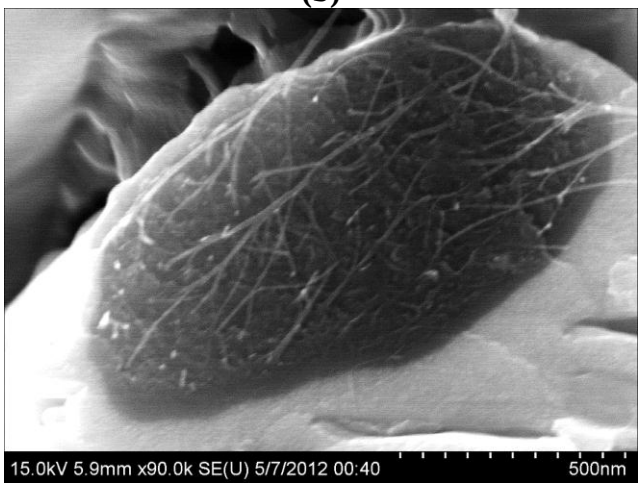

(c)

Figure 3.8 Fibers with elliptical cross-sections from bundle #3 and experiments **(a)** #40, **(b)** #38, and **(c)** #45. SEM images were acquired by Mr. Korhan Şahin.

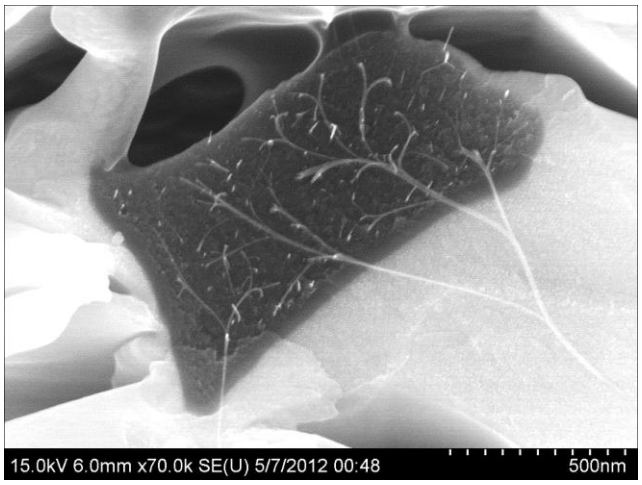

(a)

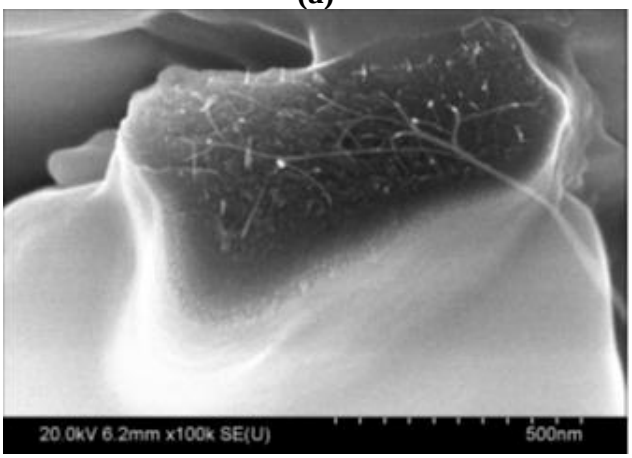

(b)

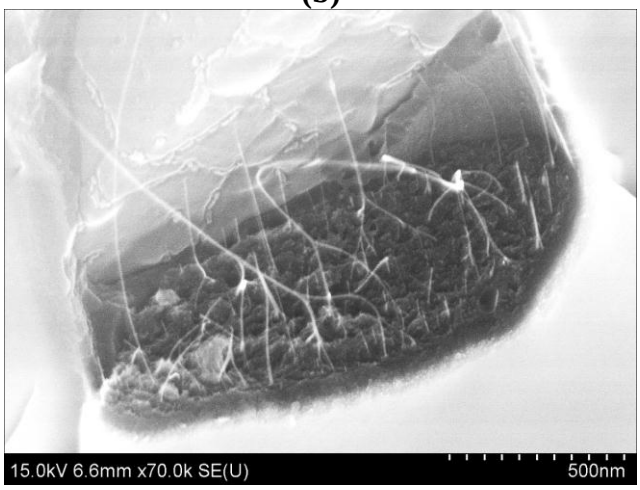

(c)

Figure 3.9 Fibers with rectangular cross-sections from bundle #3 and experiments **(a)** #46, **(b)** #27, and **(c)** #28. SEM images were acquired by Mr. Korhan Şahin.

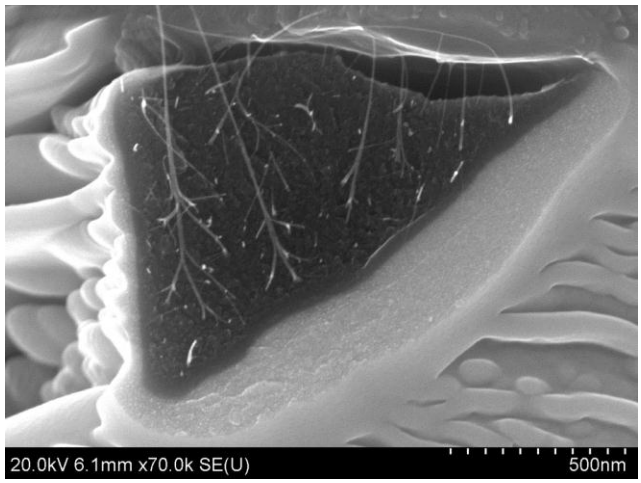

(a)

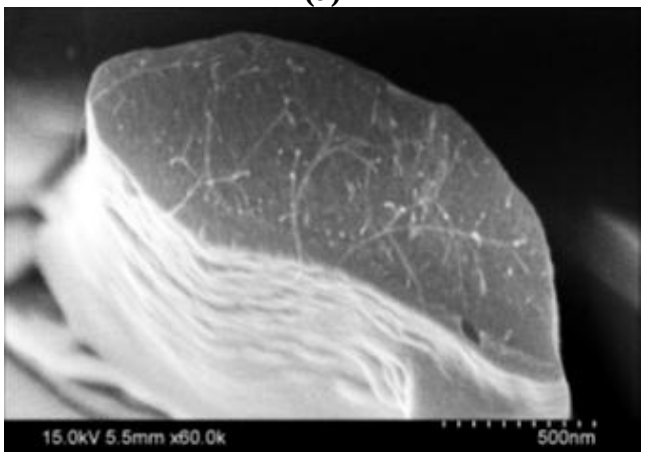

(b)

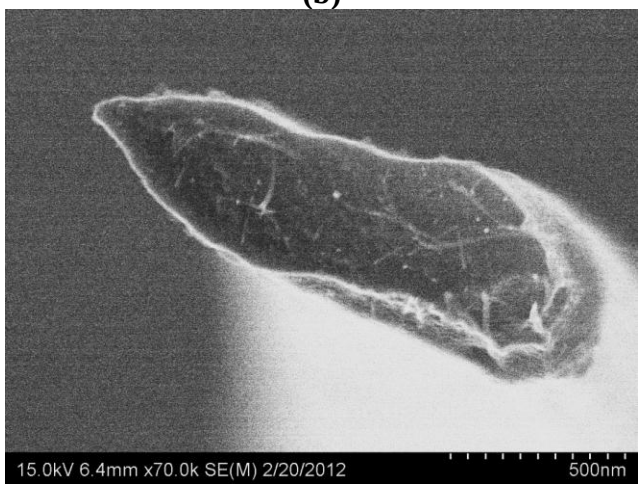

(c)

Figure 3.10 Irregular cross-sections of fibers from bundle #3 and experiments **(a)** #47, **(b)** #31, and **(c)** #37**.** SEM images were acquired by Mr. Korhan Şahin.

Although bundles #1 and #3 were manufactured under the same conditions, the fibers from bundle #3 had better mechanical properties. The 20 experiments from bundle #1 resulted in tensile strength of 3.41±0.93 GPa, Young's modulus of 228±45 GPa and Weibull characteristic strength of 4.3 GPa. The strongest fiber from bundle #1 was from experiment #12 with tensile strength of 5.66 GPa and Young's modulus of 300 GPa. The 25 experiments from bundle #3 gave an average tensile strength of 4.55±1.35 GPa, elastic modulus of 254±36 GPa, and Weibull characteristic strength of 5.07 GPa. The strongest fiber from bundle #3 was from experiment #41 with tensile strength of 7.24 GPa and a Young's modulus of 323 GPa. Overall, bundle #3 showed 33% improvement in tensile strength compared to bundle #1, and 13% increase in the value of the Young's modulus.

The majority of specimens shattered and flew away from the grips upon failure and could not be recovered to image their original fracture surfaces. The SEM images shown in Figures 3.3-3.5 and Figures 3.8-3.10 were obtained at the fiber grip. To resolve the issue of potential failure at the fiber grip, tests on fibers from bundle #3 were performed in glycerin to gather the fragments of the specimen gauge section. These experiments showed that indeed failure occurred near the Pt tabs at the specimen grip. The fused Pt layer on the fiber surface, *which was present only at the specimen grip*, is shown after fiber failure in Figure 3.11. The arrows in Figure 3.11(a) point to a thin dark layer on the fiber surface which was potentially the result of Pt diffusion into the carbon fiber. The matching side of the fiber which remained on the grip is shown in Figure 3.11(b). This thin (dark) layer for Pt/carbon could result in a small reduction in the measured tensile when Pt tabs were used. As shown in the next section, the strength measurements using epoxy gripping resulted in the same value for the highest tensile strength, but a higher average value (over a smaller set of experiments). This implies that the thin diffused Pt shell on the surface of the carbon fibers at the Pt tabs could have reduced the value of the true tensile strength and the average values for strength presented in Tables 3.1-3.4 represent a lower bound. The elastic moduli reported in Tables 3.1 and 3.3 are considered as quite accurate, within the accuracy of the loadcell calibration and the determination of the fiber cross-sectional area.

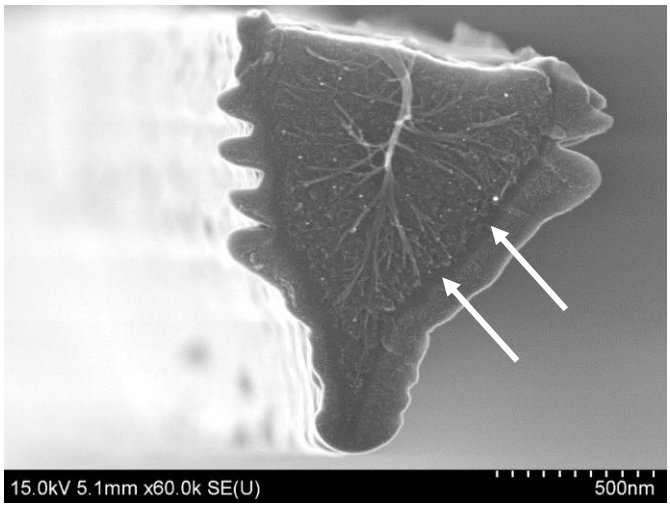

(a)

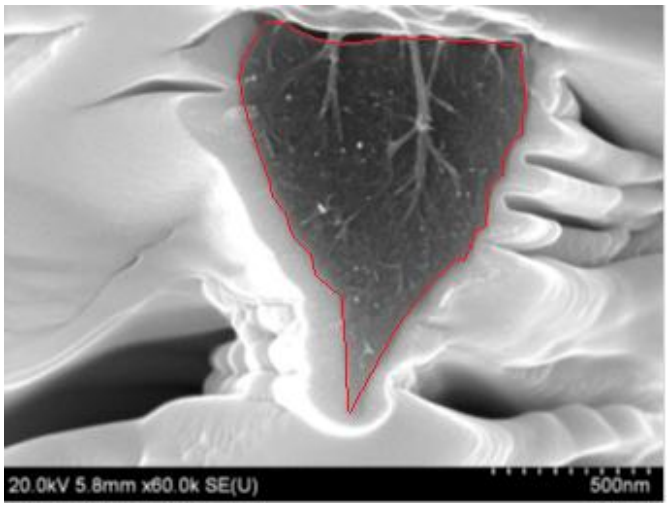

(b)

Figure 3.11 Matching cross-sections carbon fiber tested in glycerin. **(a)** Fiber side that was captured in glycerin showing the surrounding Pt tab as the mirror surface without CNTs. The white arrows point to a thin dark layer on the fiber surface which was potentially the result of Pt diffusion into the carbon fiber **(b)** Matching fracture section at the Pt tab near its fixation point to the MEMS device. The red outline shows the fiber cross-section used in the calculation of fiber strength. SEM images were acquired by Mr. Korhan Şahin.

As described in Chapter 2, more compliant epoxy/Pt grips were used to prevent damage during Pt deposition. The fibers tested by this method were isolated from bundles #2 and #3. Bundle #2 was received together with bundle #3 and, for the limited experiments that were run for this bundle, average strength and Young's modulus values were similar to those from bundle #3. The results for the fibers tested with compliant epoxy grips are given in Table 3.5. Due to the compliance of the grips, it was not meaningful to calculate the Young's modulus value from these experiments. While this data set is too small to run a Weibull analysis, the results are promising giving and average tensile strength of 5.59±1.24 GPa. In the majority of these tests the fibers did not break at the grips.

Table 3.5 Experimental results using compliant epoxy/Pt grips.

Experiment	Tensile Strength (GPa)	Gauge Length (μm)	Diameter (μm)
1	5.82	50	0.92
2	3.76	100	0.98
3	4.29	50	0.86
4	6.52	50	0.93
5	6.66	50	1.02
6	6.07	50	0.84
7	4.18	50	1.06
8	5.67	50	1.08
9	7.31	100	0.96

As a final comparison, control carbon fibers fabricated under similar conditions from pure PAN were reported to have an average strength of 3.2±0.7 GPa [67]. Experiments with single fibers from bundles #1 and #3 with rigid Pt tabs gave average strengths of 3.41±0.93 GPa and 4.55±1.35 GPa, respectively. The (limited) experiments run with compliant grips using specimens from bundles #2 and #3 resulted in an average strength of 5.59±1.24 GPa and similar maximum values as the experiments run with Pt

tabs. The CNTs clearly had a positive effect on the strength of the PAN derived carbon fibers.

3.3 Conclusions

In this Chapter, a volume corrected Weibull analysis was conducted to provide a statistical description of two sets of mechanical strength values for carbon fibers, namely 20 samples from bundle #1, and 25 samples from bundle #3. For bundle #1, the Weibull modulus and the characteristic strength are m=4.4, and σ_0 =4.13, respectively. For bundle #3, m=4.13 and σ_0 =5.07. Both sets of data followed ideal Weibull distributions for the probability estimator used in the calculations. Experiments conducted in glycerin pointed to a biasing effect of the Pt grips on the measured average strength. Such experiments revealed a thin region on the perimeter of the fibers where Pt diffusion might have occurred and caused fiber failure at the grips.

Additional experiments were run using compliant epoxy/Pt grips that prevented failure at the grips. While the number of these experiments was limited, the average tensile strength was 5.59±1.24 GPa, which is quite higher than that measured from fibers from bundle #3 using Pt grips. The largest value of strength recorded using compliant grips was 7.31 GPa, which is very comparable to the highest value measured using Pt grips. Thus, the use of Pt grips may have influenced the average value of the measured mechanical strength, but the values recorded at the high tail end of the strength distribution are quite representative of the high quality of the particular carbon fibers.

CHAPTER 4

CONCLUSIONS

The mechanical properties of PAN derived carbon fibers reinforced with CNTs were investigated. Microscale uniaxial tension tests were conducted using specially designed load cells on MEMS devices. Fibers from three different bundles, all fabricated under the same conditions were tested. Techniques were developed to isolate and test individual fibers from the bundles. Rigid grips made from Pt deposition via an FEI Dual Beam 235 FIB were used to fix the fibers onto MEMS devices for the majority of the tests that were carried out. Compliant grips made from a combination of epoxy and Pt tabs were used in experiments carried out towards the end of this study to elucidate experimental uncertainties. The mechanical strength data were analyzed using a volume corrected two-parameter Weibull probability distribution function.

The 20 experiments from bundle #1 yielded an average tensile strength of 3.41 0.93 GPa, Young's modulus of 228±45 GPa, and Weibull characteristic strength of 4.3 GPa. The 25 experiments from bundle #3 provided a tensile strength of 4.55±1.35 GPa, modulus of 254±36 GPa, and Weibull characteristic strength of 5.07 GPa. On average, bundle #3 showed a 33% improvement in strength and 13% improvement in Young's modulus over bundle #1. The strongest fibers tested from bundles #1 and #3 had tensile strengths of 5.66 GPa and 7.24 GPa, respectively. The fibers tested had an assortment of cross-sectional geometries. Inspection of the mechanical strength data did not highlight a particular geometry that resulted in consistently higher strength values.

A novel type of compliant grips made by a combination of epoxy and Pt mechanical locking tabs were used to test fibers from bundles #2 and #3 and reduce the

propensity for fiber failure at the grips. While the number of these experiments was limited, the average tensile strength was 5.59±1.24 GPa, which is quite higher than that measured from fibers from bundle #3 using Pt grips. The largest value of strength recorded using compliant grips was 7.31 GPa, which is very comparable to the highest value measured using Pt grips. Thus, the use of Pt grips may have influenced the average value of the measured mechanical strength, but the values recorded at the high tail end of the strength distribution are quire representative of the high quality of the particular carbon fibers.

When compared to control carbon fibers from pure PAN manufactured under the same conditions and tested at other labs that reported an average strength of 3.2±0.7 GPa, all carbon fibers tested in this work demonstrated higher average strengths than the control, thus showing that CNTs have a very positive effect on the tensile strength of carbon fibers.

REFERENCES

[1] E. Fitzer. "Pan-based carbon fibers-present state and trend of the technology from the viewpoint of possibilities and limits to influence and to control the fiber properties by the process parameters", *Carbon*, 27 (5), pp. 621-645, 1989.

[2] W.B. Hillig. *Proceedings of the International Conference on Reinforced Materials and Composite Technologies*, Wiesbaden, Germany, 1988.

[3] M.S. Dresselhaus, G. Dressselhaus, K. Sigihara, I.L Spain, H.A. Goldberg. *Graphite Fibers and Filaments*, Springer-Verlag, Berlin, 1988.

[4] J.L. Figneiredo *et. al*. *Carbon Fibers, Filament and Composite*. Kluwer Academic Publications, Boston, 1990.

[5] C. Pradere, C. Sauder. "Transverse and longitudinal coefficient of thermal expansion of carbon fibers at high temperatures", *Carbon*, 46 (14), pp. 1874-1884, 2008.

[6] G. Savage. *Carbon-carbon Composites*, Chapman & Hall, 1993.

[7] J.B. Donnet, O.P. Bahl, Roop C. Bansal, T.K. Wang, Carbon Fibers, Encyclopedia of Physical Science and Technology, Academic Press, New York, 2003.

[8] D.J. O'neil. "Precursors for Carbon and Graphite Fibers", *International Journal of Polymeric Materials*, 7 (3-4), pp. 203-218, 1979.

[9] J.R. White *et. al. Fibre Reinforcements for Composite Materials*, Elsevier Science Publishers, Amsterdam, 1988.

[10] J.B. Donnet *et. al. Carbon Fibers*, Marcel Dekker, New York, 1998.

[11] G.G. Tibbetts. "Carbon fibers produced by pyrolysis of natural gas in stainless steel tubes", *Appl Phys Lett*, 42 (8), pp. 666–668, 1983.

[12] J.S. Speck, M. Endo and M.S. Dresselhaus. "Structure and intercalation of thin benzene derived carbon fibers", *J Cryst Growth*, 94, pp. 834–848, 1989.

[13] C.R. Thomas, E.J. Walker. *Proceedings of the 5th Conference on Ind. Carbon and Graphite*, Society of Chemical Industry, London, p. 520, 1978.

[14] B.H. Mahin. *University Chemistry*, Addison-Wesely, Reading, Massachusetts, 1969.

[15] B.T. Kelly. "Outstanding problems in the bonding of the graphite lattice and the theory of the thermal properties of graphite", *High temperatures - High pressures*, 13 (3), pp. 245-250, 1980.

[16] E. Fitzer, L. Manocha. *Carbon Reinforcements and Carbon/carbon composite*s, Springer-Verlag, Berlin, 1998.

[17] R. Bacon, W.H. Smith. *Proceedings of the 2nd Conference on Ind. Carbon and Graphite,* Society of Chemical Industry, London, p. 203, 1965.

[18] R. Bacon. "Carbon Fibers from Rayon Precursors", *Chemistry and Physics of Carbon,* 9, p.1, 1973.

[19] A. Shindo. Report no. 217, Government Ind. Res. Inst., Osaka, Japan, 1961.

[20] L.N. Phillips, W. Watt, and W Johnson. British Patent 1110791, 1965.

[21] W. Watt and W. Johnson. *Proceedings of the 3rd Conference on Industrial Carbon and Graphite,* Society of Chemical Industry, London, p. 417, 1971.

[22] O.P. Bahl, L.M. Manocha. "Characterization of oxidised pan fibres", *Carbon*, 12 (4), pp. 417-423, 1974.

[23] Kureha Chemical Industry Co., Fr. Pat 1,465,030, 1967.

[24] S. Ōtani. "On the carbon fiber from the molten pyrolysis products", *Carbon*, 3 (1), pp. 31-34, 1965.

[25] D.D. Edie. "The effect of processing on the structure and properties of carbon fibers", *Carbon*, 36 (4), pp. 345-362, 1998.

[26] R.T.K Baker, P.S. Harris. "The Formation of Filamentous Carbon", *Chemistry and Physics of Carbon,* 14, p.83, 1978.

[27] A. Oberlin, M. Endo, T. Koyama. "High resolution electron microscope observations of graphitized carbon fibers", *Carbon*, 14 (2), pp. 133-135, 1976.

[28] A. Oberlin, M. Endo, T. Koyama. "Filamentous growth of carbon through benzene decomposition", *Journal of Crystal Growth*, 32 (3), pp. 335-349, 1976.

[29] T. Koyama, M.T. Endo. "Method for Manufacturing Carbon Fibers by a Vapor Phase Process," Japanese Patent 1982-58, 966, 1983.

[30] M. Hatano, T. Ohsaki, K. Arakawa. "Graphite Whiskers by New Process and Their Composites, Advancing technology in Materials and Processes", Science *of Advanced Materials and Processes,* 30, pp. 1467-1476, 1985.

[31] E. Hammel, X. Tang, M. Trampert, T. Schmitt, K. Mauthner, A. Eder, P. Pötschke. "Carbon nanofibers for composite applications", *Carbon*, 42 (5-6), pp. 1153-1158, 2004.

[32] M. Minus, S. Kumar. "The processing, properties, and structure of carbon fibers", *Journal of the Minerals*, 57 (2), pp. 52–58, 2005.

[33] G.J. Capone. "Wet-spinning technology", In: *Acrylic Fiber Technology and Applications*, ed. J.C. Masson, Marcel Dekker, New York, pp. 69-103, 1995.

[34] D.D. Edie, R.J. Diefendorf. "Carbon fiber manufacturing". In: *Carbon-Carbon Materials and Composites*, eds. J. D. Buckley and D. D. Edie. Noyes Publications. Park Ridge, NH, pp. 19-37, 1993.

[35] V.B. Gupta and V.K. Kothari. *Manufactured Fibre Technology*, Chapman & Hall, London, 1997.

[36] M.J. Ram, J.P. Riggs. "Process for production acrylic filaments", U.S. Patent 3 657 409, 1972.

[37] L.H. Peebles. *Carbon Fiber – Formation, Structure, and Properties*, CRC Press, Boca Raton, LA, 1995.

[38] E. Fitzer, D.J. Müller. "The influence of oxygen on the chemical reactions during stabilization of pan as carbon fiber precursor", *Carbon*, 13 (1), pp.63-69, 1975.

[39] A.K. Fiedler, E. Fitzer, and F. Rozploch. *Proceedings of 11th Biennial Conf. on Carbon*, p. 261, 1973.

[40] E. Fitzer, W. Frohs, M. Heine. "Optimization of stabilization and carbonization treatment of PAN fibres and structural characterization of the resulting carbon fibres", *Carbon*, 24 (4), pp. 387-395, 1986.

[41] T. Matsumoto. "Mesophase pitch and its carbon fibers", *Pure Applied Chemistry*, 57 (11), pp. 1553-1562, 1985.

[42] R. Moreton, W. Watt, W. Johnson. "Carbon fibres of high strength and high breaking strain", *Nature*, 213, pp.690-691, 1967.

[43] E. Fitzer, W. Frohs. "The influence of carbonization and post treatment conditions on the properties of PAN-based carbon fibers". *Proceedings of the International Carbon Conference*, Newcastle, U.K., pp. 18-23, 1988.

[44] S.C. Bennett, D.J. Johnson, W. Johnson. "Strength-structure relationships in PAN-based carbon fibres", 18 (11), pp. 3337-3347, 1983.

[45] D.J. Johnson. "Structure property relationships in carbon fibers", *Journal of Physics D: Applied Physics*, 20 (3), pp. 287-291, 1987.

[46] M.M. Treacy, T.W. Ebbesen, and J.M. Gibson. "Exceptionally high Young's modulus observed for individual carbon nanotubes", *Nature*, 381, pp.678-680, 1996.

[47] B. Yakobson. "Mechanical properties of carbon nanotubes". *Topics in Applied Physics*, 80, pp. 287-329, 2001.

[48] R.E. Smalley, et al. "Crystalline ropes of metallic carbon nanotubes", *Science*, 273, pp. 483-487, 1996.

[49] J.W.G. Wildoer, L.C. Venema. A. G. Rinzler, R. E. Smalley, C. Dekker, "Electronic structure of atomically resolved carbon nanotubes, *Nature*, 391, pp. 59–62, 1998.

[50] T. W. Odom, J. L. Huang, P. Kim, C. M. Lieber. "Atomic structure and electronic properties of single-walled carbon nanotubes", *Nature*, 391, pp. 62–64, 1998.

[51] M.S. Dresselhaus, P.C. Eklund. “Photons in carbon nanotubes”, *Advances in Physics*, 49 (6), pp.705-814, 2000.

[52] J. Hone. "Phonons and Thermal Properties of Carbon Nanotubes", *Topics in Applied Physics*, 80, pp. 273-287, 2001.

[53] M.S Dresselhaus, P. Avouris. "Introduction to Carbon Materials Research." *Topics in Applied Physics*, 80, pp. 1-9, 2001.

[54] G.D. Li, Z.K. Tang, N. Wang, J.S. Chen. “Structural study of the 0.4-nm single-walled carbon nanotubes aligned in channels of AlPO4-5 crystal”, *Carbon*, 40 (6), pp. 917-921, 2002.

[55] D.A. Walters, et al. “Elastic strain of freely suspended single-wall carbon nanotube ropes”, *Appied Physics Letters*, 74 (25), pp. 3803-3805, 1999.

[56] G. Gao, T. Cagin, W.A. Goddard III. “Energetics, Structure, mechanical and vibrational properties of single-walled carbon nanotubes Nanotechnology, 9, pp. 184-191, 1998.

[57] J. Cumings, W. Mickelson, A. Zettl. “Simplified synthesis of double-wall carbon nanotubes”, *Solid State Communications*, 126 (6), pp. 359-362, 2003.

[58] B. Yakobson. "Mechanical Properties of Carbon Nanotubes". *Topics in Applied Physics*, 80, pp. 287-329, 2001.

[59] H. W. Kroto, J. R. Heath, S. C. O’Brien, R. F. Curl, R. E. Smalley. “C_{60}: Buckminsterfullerene”, *Nature*, 318, pp. 162–163, 1985.

[60] S. Iijima. “Helical microtubules of graphitic carbon”, *Nature*, 354, pp. 56-58, 1991.

[61] S. Iijima, T. Ichihashi, “Single-shell carbon nanotubes of 1-nm diameter”, *Nature*, 363, pp. 603-605, 1993.

[62] D. S. Bethune, C. H. Kiang, M. S. de Vries, G. Gorman, R. Savoy, J. Vazquez, R. Beyers. “Cobalt-catalysed growth of carbon nanotubes with single-atomic-layer walls”, *Nature*, 363, pp. 605-607, 1993.

[63] H.G. Chae, T.V. Sreekumar, T. Uchida, S. Kumar. “A comparison of reinforcement efficiency of various types of carbon nanotubes in polyacrylonitrile fiber”, *Polymer*, 46 (24), pp.10925–10935, 2005.

[64] H.G. Chae, M.L. Minus, A. Rasheed, S. Kumar. “Stabilization and carbonization of gel spun polyacrylonitrile/single wall carbon nanotube composite fibers”, *Polymer*, 48 (13), pp.3781–3789, 2007.

[65] H.H. Ye, H. Lam, N. Titchenal, Y. Gogotsi, F. Ko. “Reinforcement and rupture behavior of carbon nanotubes-polymer nanofibers”, *Applied Physics Letters*, 85(10), pp. 1775-1777, 2004.

[66] S. Liu, L. Tan, D. Pan, Y. Chen. “Gel spinning of polyacrylonitrile fibers with medium molecular weight”. *Polymer International*, 60, pp. 453–457, 2011.

[67] H.G. Chae, Y.H. Choi, M. L. Minus, S. Kumar. “Carbon nanotube reinforced small diameter polyacrylonitrile based carbon fiber”, Composites *Science and Technology,* 69 (3-4), pp.406-413, 2009.

[68] http://www.toraycfa.com/pdfs/T300DataSheet.pdf

[69] http://www.nist.gov/public_affairs/practiceguides/NIST%20SP960-19.pdf

[70] F. Inam. "Dimethylformamide: An effective dispersant for making ceramic-carbonnanotube composites" *Nanotechnology,* 19, p. 195710, 2008.

[71] R. Poyato. "Aqueous colloidal processing of single-wall carbon nanotubes and their composites with ceramics" *Nanotechnology,* 17, pp. 1770-1770, 2006.

[72] M. Naraghi, I. Chasiotis, Y. Dzenis, Y. Wen, H. Kahn. “Mechanical deformation and failure of electrospun polyacrylonitrile nanofibers as a function of strain rate”, *Applied Physics Letters,* 91, p. 151901, 2007.

[73] M. Naraghi, I. Chasiotis, Y. Dzenis, Y. Wen, and H. Kahn, “Novel Method for Mechanical Characterization of Polymeric Nanofibers”, *Review of Scientific Instruments*, 78, p. 085108, (2007)

[74] S.N. Arshad, M. Naraghi, I. Chasiotis. “Strong Carbon Nanofibers from Electrospun Polyacrylonitrile”, *Carbon*, 49 (5), pp. 1710-1719, 2011.

[75] T. Ozkan, M. Naraghi, I. Chasiotis. “Mechanical Properties of Vapor Grown Carbon Nanofibers”, *Carbon* 48 (1), pp. 239-244, 2010.

[76] M. Naraghi, S. Arshad, I. Chasiotis. “Molecular Orientation and Mechanical Property Size Effects in Electrospun Polyacrylonitrile Nanofibers”, *Polymer*, 52, pp. 1612-1618, 2011.

[77] M. Naraghi, I. Chasiotis, “Optimization of Comb-driven Devices for Mechanical Testing of Polymeric Nanofibers Subjected to Large Deformations”, *Journal of Microelectromechanical Systems*, 18 (5), pp. 1032-1046, 2009.

[78] W. Weibull. “A Statistical Theory of the Strength of Materials”, Royal Swedish Institute for Engineering Research, Stockholm, Sweden, 1939.

[79] M.F. Ashby, D.R.H. Jones. *Engineering materials 2: An Introduction to Microstructures, Processing and Design*, Pergamon Press, Oxford, England, 2005.

[80] B. Bergman. “On the estimation of the Weibull modulus”, *Journal of Materials Science Letters*, 3 (8), pp. 689-692, 1984.

[81] M.R. Gurvich, A.T. DiBenedetto, A. Pegoretti. “Evaluation of the statistical parameters of a Weibull distribution”, Journal *of Materials Science*, 32 (14), pp. 3711-3716, 1997.

[82] K. Trustrum, A.D.S. Jayatilaka. “On estimating the Weibull Modulus for a brittle material”, Journal of Material Science, 14 (5), pp. 1080-1804, 1979.